Determination of Metamorphic Temperatures of the Raspas Complex, Ecuador, Using Zr-in-Rutile Thermometry

Helen Hutchinson

Advised by Dr. Sarah Penniston-Dorland

GEOL394

November 25, 2024

Abstracts

Abstract

The thermobarometric method defined by the zircon-quartz-rutile system uses the concentration of substituted Zr for Ti in rutile within metamorphic rocks to calculate a peak temperature estimate for the metamorphic conditions in multiple tectonic settings, including subduction zones. Zr-in-rutile thermometry can be applied to rocks recovered from the Raspas Complex, a metamorphic accretionary unit located in southern Ecuador that was formed in the beginning stages of the Andean Orogeny at 130 Ma in the Early Cretaceous. Data on the Zr in rutile concentrations of two eclogites and two blueschists were collected using EPMA. Eclogite samples display temperatures ranging from 559° to 644°C at pressures of 1.6 to 1.8 GPa, while blueschist samples display temperatures of 538° to 548°C at pressures of 1.4 to 1.6 GPa. These calculations are consistent within uncertainty with previous estimates made with Fe-Mg exchange garnet-clinopyroxene thermometry that estimated temperature ranges from 600-700°C at 1.6-1.8 GPa for the eclogites and 550-650°C at 1.4-1.6 GPa for the blueschists. Additionally, matrix rutile and rutile included in garnet were measured and evaluated to determine if there is a significant difference in Zr concentration and, therefore, recorded peak temperatures. There does not appear to be any connection between recorded temperature and whether rutile is in garnet or matrix. There also appears to be no correlation between Zr concentration and location within a single rutile crystal. Temperature estimates such as those in this study provide further understanding of the thermal conditions of subduction zones and how they impact the processes occurring there.

Plain Text Abstract

The regions on Earth where two tectonic plates converge and create a subduction zone are subject to high pressure and temperature conditions, which cause rocks to undergo metamorphism. These conditions can be estimated by examining elements in minerals within the rocks, including Zr in the mineral rutile. The Raspas Complex in Ecuador is a 130-million-year-old unit that contains metamorphic rocks with accessory rutile, allowing for the usage of the Zr-in-rutile thermometer. This complex is related to the mountain-building event that created the Andes mountains and is responsible for the volcanic and seismic activity seen in the region today. Measuring the Zr concentration with an electron probe and plugging the results into the thermometer reveals temperatures consistent with previous temperature estimates based on other mineral systems. The temperature recorded by the rutile does not seem to be affected by the location of the rutile grain in the rock. This study will help us understand the temperature conditions deep underground in subduction zones, which will make it easier to predict changes in the temperature that affect volcanoes and earthquakes.

Table of Contents

Introduction

Subduction zones are some of the most important regions in the cycle of plate tectonics, as they are essential to the recycling of the crust into the mantle. Regions around subduction zones are also home to some of the world's largest and most populated cities, which are heavily affected by the intense earthquakes and volcanism that occur there. The pressure and temperature conditions deep in the mantle during subduction are not fully understood, as there are only a few methods of quantifying them. One such method is through the study of metamorphic rocks, which are readily found at subduction zones.

By examining the chemical composition of subduction zone metamorphic rocks, the pressure and temperature conditions that caused their metamorphism can be estimated. There are several methods of geothermobarometry, but all have the same goal of understanding conditions at the various tectonic settings in which metamorphism occurs. Regional metamorphism (and specifically subduction metamorphism) occurs in tectonically active areas on Earth. Certain tectonic events that are common near subduction zones, such as volcanoes and earthquakes, are related to the temperatures under the Earth's surface. The temperature of a subduction zone has a strong impact on the production of magma below volcanic arcs, including volume and composition (van Keken & Wilson, 2023). Earthquakes along the plate boundary are impacted by processes like fluid production, the rate of which is temperature dependent (van Keken & Wilson, 2023). Gaining a greater understanding of subduction zone temperatures allows us to investigate the causes of these natural disasters and when and how they occur.

Many numerical models have been made to study the conditions of subduction zones across the world. When compared to pressure-temperature conditions estimated based on rocks using geothermobarometry, the models are generally consistent with the estimates at high pressures. However, at lower pressures and overall, the rocks display higher temperatures than the models at a given pressure, as seen in **Figure 1** (Penniston-Dorland et al., 2015). It is unclear if the discrepancy lies in the geothermobarometry or in the calibration of the models. By studying the temperatures determined through sample analysis, we can better evaluate the differences between the estimates and the predictions and either adjust our methods of geothermobarometry or create better subduction zone models that more accurately represent what happens during subduction.

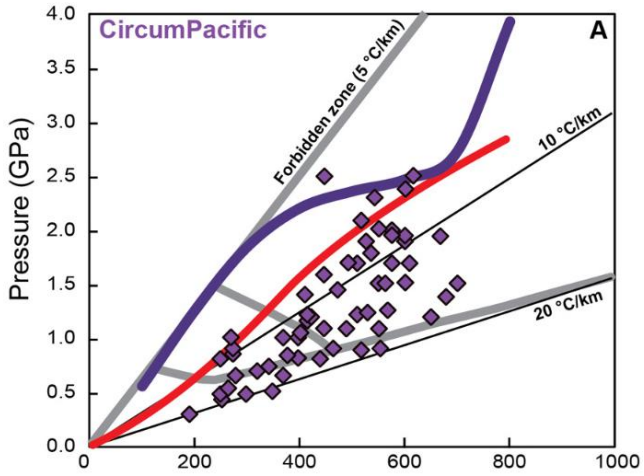

Figure 1: P-T estimates for subduction zones around the Pacific Plate. Estimates based on numerical models are shown as solid red (Gerya et al., 2002) and purple (Syracuse et al., 2010) lines. Estimates based on geothermobarometry of exhumed metamorphic rocks are shown as purple diamonds. From Penniston-Dorland et al. (2015).

Rutile and the Zr-in-Rutile Thermometer

Rutile (TiO_2), a common accessory mineral in many types of metamorphic rocks, offers insight into the elevated temperatures that cause metamorphism to occur. During metamorphism, Zr from other phases in the rock can substitute for Ti. This is possible due to the shared +4 charge on both ions, but the larger ionic radius of Zr makes this substitution more difficult at lower temperatures. Therefore, the concentration of trace Zr within rutile increases as temperature increases. This relationship allows the calculation of a thermometer to estimate the peak temperature a rock experienced during the metamorphic process.

Zr-in-rutile thermometry is a system initially developed by Zack et al. (2004) based on the equilibrium system:

$$SiO_2 + ZrO_2 = ZrSiO_4.$$

This reaction represents the interaction between quartz, rutile with substituted Zr, and zircon. While the original thermometer proposed by Zack et al. (2004) was relatively simple, later researchers refined the thermometer to include corrections for pressure and to be a better fit for experimental data (Tomkins et al., 2007; Kohn, 2020).

Models indicate that rutile grains form at high temperatures during metamorphism, making them useful for determining peak temperatures. As the rock cools and is uplifted, the rutile may re-equilibrate, decreasing the Zr concentration. This will cause the recorded temperature to decrease. However, this re-equilibration has been found to only affect the outer edges of the rutile grains, around 10-20 μm (Kohn, 2020). Therefore, peak temperatures can still be determined by measuring the Zr concentrations in the center of

the grains. This is an advantage over methods such as Fe-Mg exchange thermometers, which are more prone to resetting during uplift. Because of this, temperature estimates using Zr-in-rutile thermometry may be different than other methods.

Goals

The overall goal of this study is to measure the Zr content in rutile grains in eclogites and blueschists from the Raspas Complex in southern Ecuador. The Zr concentration will then be used to estimate the peak temperatures experienced by these rocks during their metamorphism. Other questions that will be explored include:

- How do temperature estimates based on Zr-in-rutile compare to other thermobarometric methods?
- Is there a relationship between rock type and temperature?
- Do rutile grains in garnet porphyroblasts record different Zr concentrations (and therefore temperatures) than grains in the matrix?

Background

Geologic Background

Subduction zones occur at convergent plate boundaries, where denser oceanic crust dives beneath a less dense plate of either continental or oceanic crust and sinks into the mantle. Due to the lower temperatures of old oceanic crust and the high speed of the subducting plate, which is faster than the speed of conduction, subduction zones are generally colder than the lithosphere around them at similar depths. The low temperatures and high-pressure conditions displayed in subduction zones make them a unique tectonic setting that creates distinctive rock types. A typical subduction zone is shown in **Figure 2**.

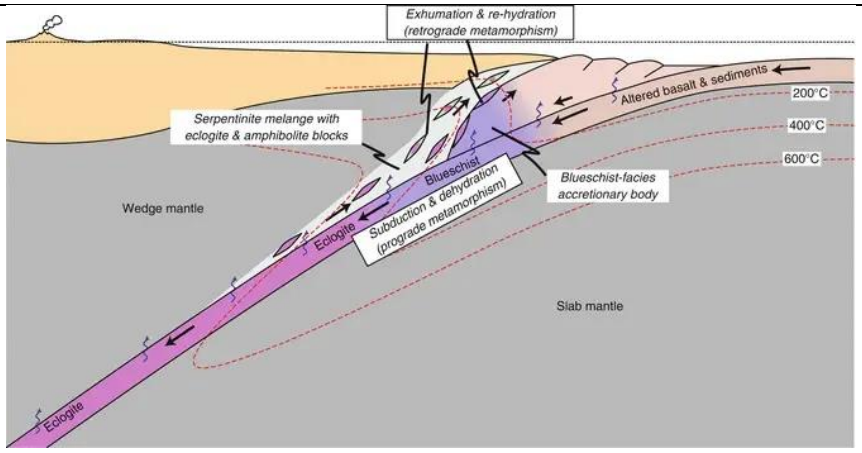

Figure 2: A diagram of a typical ocean-continent subduction zone, showing how basalt metamorphoses into blueschist and eclogite as depth increases. Isotherms are shown as red dashed lines. From Ueda (2016).

Eclogite is a metamorphic rock composed of primarily omphacitic pyroxene and iron-rich garnet. Other minerals, including quartz, micas, rutile, and kyanite, are also common. Protoliths are basaltic oceanic crust. Eclogite is commonly formed during subduction, where the subducted slab is metamorphosed due to high-pressure conditions. It gives its name to eclogite facies rocks, which are defined by their high (>1.2 GPa) pressure and moderate temperatures (>400-500°C) and includes other rock types, including gneisses and metapelites (Winter, 2013).

Blueschist is a metamorphic rock defined by a high percentage of glaucophane, but may also contain minerals like lawsonite, garnet, and epidote. The glaucophane grains align under pressure, leading to a foliated, schistose texture. Blueschist protoliths are basaltic. They also form in subduction zones due to high-pressure conditions, though typically at a shallower depth than eclogites. The blueschist facies is characterized by rocks metamorphosed at pressures of >0.6 GPa and temperatures between ~200° and ~500°C (Winter, 2013). **Figure 3** shows the generally accepted P-T conditions for blueschist, eclogite, and other common metamorphic facies.

Blueschist and eclogite are both classified as high-pressure rocks, with eclogite displaying higher temperatures. In subduction zones, it is common to see blueschist facies rocks transform to eclogite facies rocks as depth increases. When uplifted, blueschist and eclogite are often found associated with each other, suggesting their common origin as subduction zone metamorphic rocks.

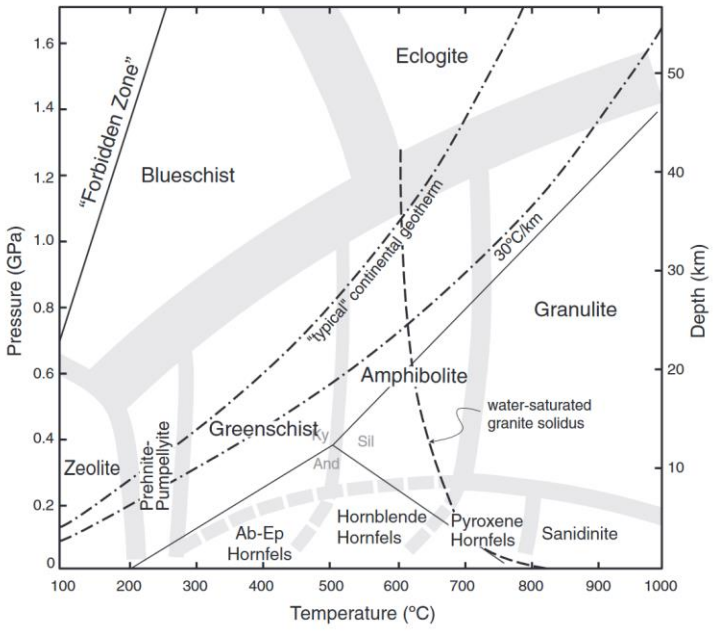

Figure 3: Characteristic P-T conditions for metamorphic facies. Eclogite and blueschist are shown at the top of the diagram, indicating their status as high-pressure metamorphic rocks. From Winter (2013).

Ecuador is located at the boundary of the Nazca and South American plates, where a subduction zone has formed. The Andes Mountains are an orogenic belt formed by this

subduction. The Raspas Complex, located in southwestern Ecuador, consists of metamorphic rocks with mafic and sedimentary protoliths. Greenschists, blueschists, eclogites, metapelites, and serpentinites are all present, as shown in **Figure 4**. It is believed to be a tectonic mélange resulting from subduction and subsequent accretion of oceanic crust. This complex is exposed in the coastal lowlands to the west of the Andes. Subduction in the region initiated during the late Jurassic (Jaillard et al., 1990). K-Ar and Lu-Hf dating of several rocks determine that the complex cooled during the early Cretaceous (John et al., 2010). This age is consistent with the first phase of the Andean Orogeny. The eclogites of the Raspas were previously believed to have formed from subducted oceanic plateau basalts, while the lower metamorphic grade rocks, including blueschists, were believed to have typical mid-ocean ridge basalt (MORB) protoliths (Bosch et al., 2002). More recent studies into the trace-element geochemistry of the rocks suggest the entire unit represents an ophiolite sequence consisting of a mixture of MORB and seamount protoliths (John et al., 2010). Mineralogical studies indicate that the blueschists may have overprinted an earlier, higher-pressure mineral assemblage. Due to the dense vegetation, there are few outcrops of the Raspas Complex.

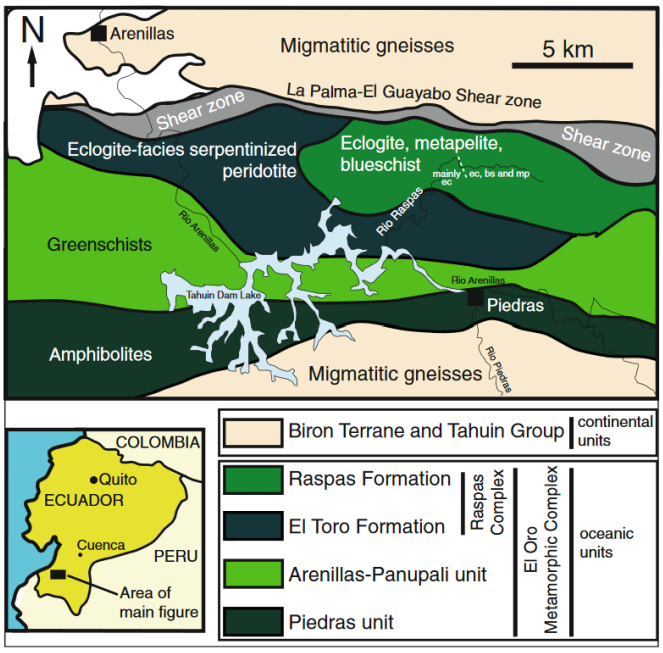

Figure 4: A geologic map showing an overview of the major formations and rock types found in the Raspas Complex and surrounding units. The rocks in this study were taken from along the marked Rio Raspas. From John et al. (2010).

Samples

Samples were acquired by Timm John from boulders along the Rio Raspas, nine of which were sent to the University of Maryland. For this study, four of these samples were analyzed. The samples were all recovered from a small geographic range within the complex. Coordinates were provided for six of the nine samples as well as for several other samples mentioned in John et al. (2010), shown in **Figure 5**. The set of samples includes

both eclogite and blueschist compositions, allowing a comparison of peak temperatures for the two rock types.

Figure 5: Google Earth satellite image showing the geographic coordinates for the sample locations from John et al. (2010). The reservoir (Represa Tahuin) shown here is the same as the one shown in **Figure 4** (labeled "Tahuin Dam Lake").

Sample SEC 43-03 (**Figure 6**) is a typical eclogite with a largely omphacitic matrix and euhedral garnet porphyroblasts ranging from 0.5-5 mm in diameter. Other minerals include green amphibole, phengite, quartz, and rutile. Zircon is also present as an accessory mineral, though it is difficult to spot even through a microscope.

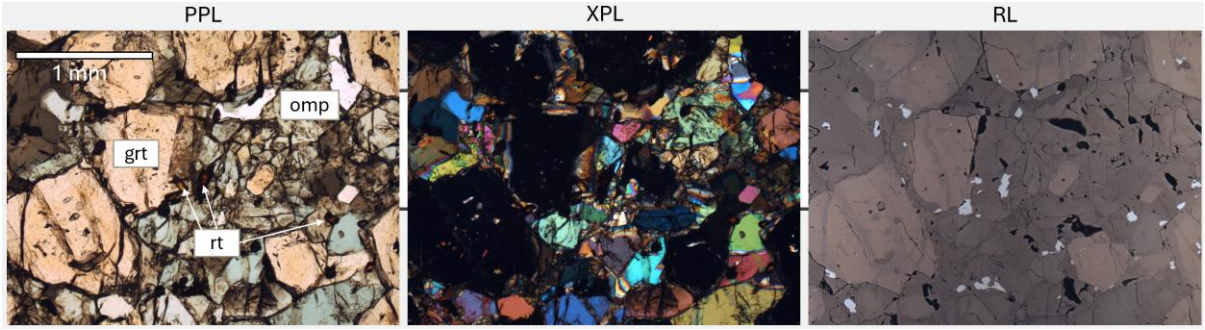

Figure 6: Photomicrographs of sample SEC 43-03 with 50x magnification. Plane polarized, cross polarized, and reflected light are shown. Omphacite, garnet, and rutile are labeled.

Sample SEC 15-02 (**Figure 7**) is a blueschist displaying strong foliation. The matrix is fine, largely made of small crystals of glaucophane and other amphiboles. Garnet porphyroblasts are small, the largest being ~1 mm across. Rutile crystals in the matrix are often rimmed by other titanium-bearing minerals. Phengite, quartz, and zircon are also present.

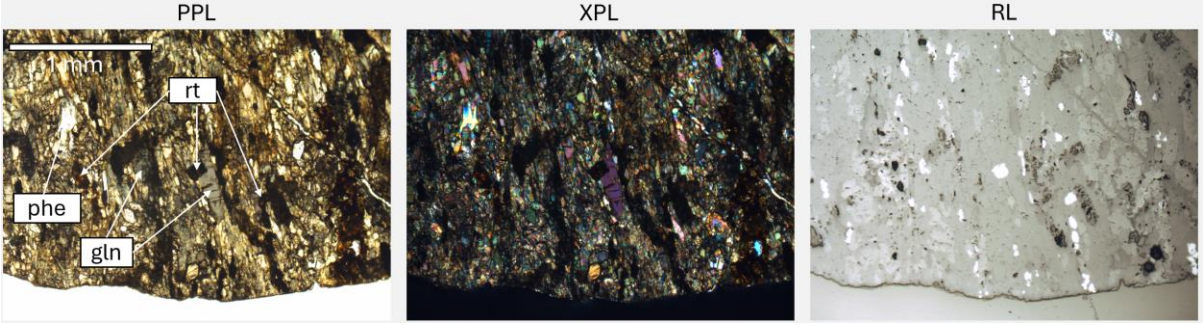

Figure 7: Photomicrographs of sample SEC 15-02 with 50x magnification. Plane polarized, cross polarized, and reflected light are shown. Glaucophane, phengite, and rutile are labeled.

Sample SEC 29-2 (**Figure 8**) is an eclogite containing smaller garnet porphyroblasts, the largest around 1 mm in diameter. The matrix is mostly omphacite, but also contains glaucophane and other blue minerals, giving the thin section a more turquoise color than green. Quartz, phengite, and rutile are also present, with one rutile crystal nearly 1 mm long. Zircon is present as a minor accessory mineral.

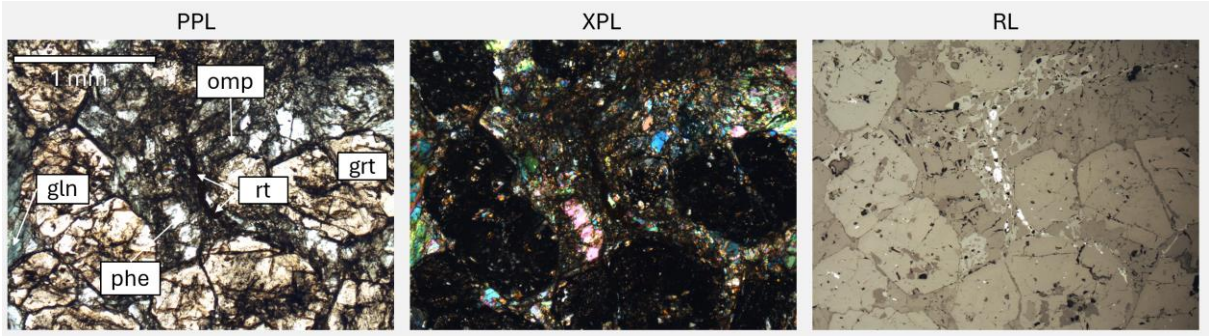

Figure 8: Photomicrographs of sample SEC 29-2 with 50x magnification. Plane polarized, cross polarized, and reflected light are shown. Omphacite, glaucophane, garnet, phengite, and rutile are labeled.

Sample SEC 16-01 (**Figure 9**) is a blueschist with a very fine matrix that demonstrates crenulation cleavage. Glaucophane and other amphiboles are present in the fabric and as larger grains. Several large garnet porphyroblasts are present, ranging 1-4 mm in diameter. The pattern of inclusions within the garnet crystals indicates that the porphyroblasts formed syntectonically. Like sample 15-02, rutile in the sample is often surrounded by other titanium-bearing phases. Phengite, quartz, and zircon are also present.

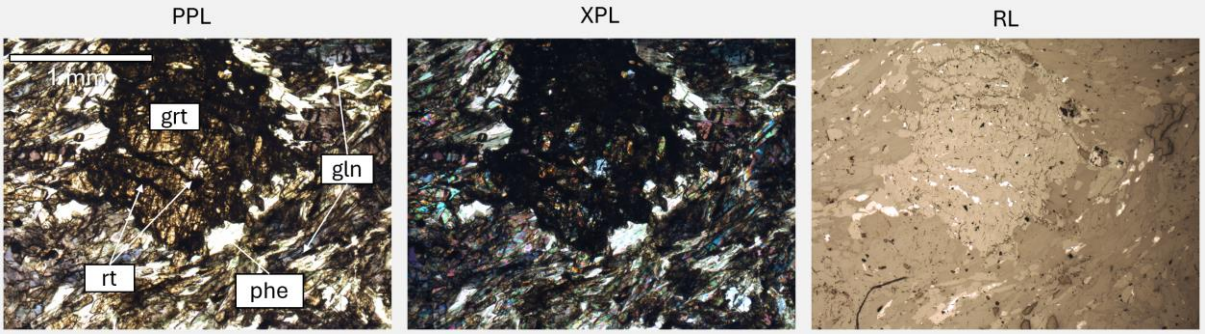

Figure 9: Photomicrographs of sample SEC 16-01 with 50x magnification. Plane polarized, cross polarized, and reflected light are shown. Glaucophane, garnet, phengite, and rutile are labeled.

Past Analyses

Previous geothermobarometric analysis by John et al. (2010) estimated a range of pressure-temperature conditions for the eclogite and blueschist samples using two different thermometers. With the Fe-Mg exchange garnet-clinopyroxene thermometer, the estimated temperature range for the blueschists was 550-650°C at 1.4-1.6 GPa. The eclogites displayed a range from 600-700°C at 1.6-1.8 GPa. Using the garnet-phengite thermometer, the calculated temperatures for the blueschists were 500-600°C, while those of the eclogites were 550-680°C. These results are shown in **Figure 10**. These estimates were consistent with earlier estimates of 590° ± 20°C at 1.3 ± 0.3 GPa (Feininger, 1980) and 550-600°C at 1.8 GPa (Gabriele, 2002) for Raspas Complex eclogites. The temperatures of the blueschists are higher than the typically understood conditions, which could related to overprinting.

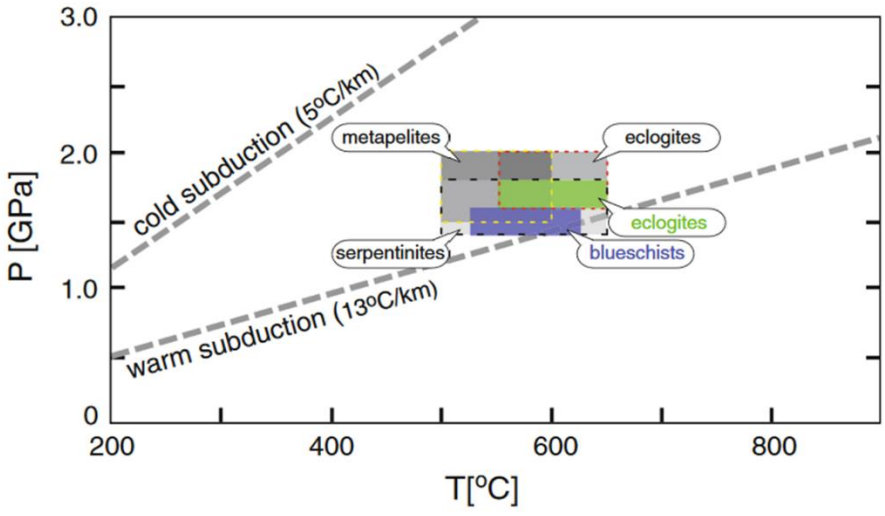

Figure 10: P-T estimates for the samples by John et al. (2010), shown in the blue and green boxes. Gray boxes represent data from previous studies of the Raspas Complex. From John et al. (2010).

During the summer of 2023, high school student Srinidhi Guruvayurappan, working under Dr. Penniston-Dorland, performed Zr-in-rutile analysis on three of the nine samples. All of those samples were eclogites: SEC 27-1, SEC 43-1, and SEC 50-01. She estimated temperatures for a pressure range of 1.3-1.8 GPa. Sample SEC 27-1 had temperatures in a range of 534-555°C, SEC 43-1 a range of 635-657°C, and sample SEC 50-1 a range of 550-570°C (see *Appendix 4*).

Hypotheses

Null: Temperatures determined using Zr-in-rutile thermometry will be consistent (within uncertainty) with those estimated by John et al. (2010).

Alternative: Temperatures determined using Zr-in-rutile will be higher or lower than previous estimates.

Secondary Null: Temperature estimates determined through Zr-in-rutile geothermometry for both eclogites and blueschists will be the same within uncertainty.

Secondary Alternative: The eclogite samples will display higher temperatures than the blueschists.

Methods

Petrography

The samples were each examined under plane polarized, cross polarized, and reflected light on a Nikon Eclipse LV100 Polarizing microscope in the Microscope Lab at the University of Maryland. Locations containing rutile grains were located and marked on a printed copy of a scan of each thin section. I obtained photomicrographs using the attached QImaging Micropublisher 5.0-RTV Camera of each of these locations to aid in locating them while using the electron microprobe. Rutile found in the matrix and as inclusions in garnet were both noted. Only rutile grains that were visible in reflected light were considered to ensure measurability using the electron probe. Twenty-five locations on SEC 43-03 were marked, each of which contained multiple rutile crystals large enough for probe analysis. Fifteen locations were noted for SEC 16-1 and SEC 29-2 and 13 for SEC 15-02 due to the concentration of rutile in each area.

Electron Probe Microanalysis

The samples were analyzed using a JEOL8900R electron microprobe at the AIM Lab in the Maryland Nanocenter at the University of Maryland. Five spectrometers were optimized for wavelength-dispersive spectrometry (WDS) analysis of various elements: #1 for Ti, Fe, Cr, Mn, Ta, and V; #2 for Zr; #3 for Zr and Nb; #4 for Zr; and #5 for Al and Si. A set of standards was used to calibrate the spectrometers for these elements: a synthetic rutile for Ti, a chromite for Cr and Al, niobium metal for Nb, tantalum metal for Ta, vanadium metal for V, a synthetic zircon for Zr and Si, and an ilmenite for Fe and Mn (as Mn can substitute for Fe in solid solution). The probe was operated with an accelerating voltage of 20 keV, a current of 120 nA, and a beam diameter of 1 μm. The Zr count time varied for each spectrometer,

with #2 and #4 measuring for 300 s at the peak and 150 s on each side (the background), and #3 measuring for 240 s at the peak and 120 s on each side. The Zr detection limit was 25 ppm at the one sigma level. When the samples are analyzed, 5 analyses are first run on a sample with known Zr concentration, K-13-02. The Zr concentration of standard K-13-02 was known to be 308 ± 45 ppm. All values measured on the probe for the standard fell within this uncertainty. Raw x-ray data was corrected using ZAF correction for atomic number (Z), absorption (A), and fluorescence excitation (F). WDS analyses for the sample were reported as wt% oxides. Electron-dispersive spectrometry (EDS) spectra were also obtained to confirm the presence of quartz and zircon grains in the samples as required to define the system.

Once measured, the data was organized to clear out any unusable measurements. The criteria for an analysis to be kept were that the total wt.% must be 100% ±2%, the wt.% TiO_2 must be above 97%, and the wt.% FeO must be below 1%. This eliminates any measurements mistakenly taken from minerals other than rutile. Data were also excluded if the uncertainties rendered the measurements unusable, such as one case with a 1σ uncertainty of 1322.9 wt.% ZrO_2.

Estimating Temperature

Once measured and analyzed, Zr concentrations were used to calculate temperature estimates using a modified Zr-in-rutile thermometer in which T represents the temperature in °C, P represents pressure in bars, C represents the concentration of Zr in ppm, and R represents the ideal gas constant 8.314 J/mol·K (Kohn, 2020):

$$T = \frac{71360 + 0.378 \times P - 0.130 \times C}{130.66 - R \times \ln(C)} - 273.1$$

Results

SEC 43-03

The Zr concentrations of rutile were analyzed in 47 locations on sample SEC 43-03. Of the 47 analyses, six were excluded. The wt% ZrO_2 of the 41 remaining analyses were converted to ppm Zr and plotted. These concentrations were then averaged using the mean maximum Zr technique (Penniston-Dorland et al., 2018). This technique is performed by averaging a population of analyses with the highest Zr concentrations. This population must include at least 4 analyses including the highest value (within uncertainty) to be considered to represent the peak temperature of the overall rock (Harvey et al., 2020). Uncertainty for the mean maximum Zr concentration was found by taking the standard deviation of the concentrations used in the mean max Zr calculation and doubling it to find 2σ. Graphs displaying this process for all samples can be found in *Appendix 3*. The population used for this sample was based on the mean of the 12 highest analyses. The error envelope for the mean max Zr value includes all but three analyses. This provided a value of 236 (±31) ppm Zr. An upper quartile mean, which is also often used for Zr-in-rutile

thermometry (Tomkins et al. 2007), was also calculated for comparison, yielding a value of 241 ppm Zr, which falls within the uncertainty of the mean max value.

The peak temperature of the rock was calculated using this mean max Zr value at a range of pressures from 1.4 to 1.8 GPa based on those calculated by John et al. (2010). This yielded a temperature range of 626° to 644°C ±12°C, shown in **Figure 12**.

SEC 15-02

Fifty-three analyses were collected on sample SEC 15-02. Five analyses were excluded. The remaining 48 analyses underwent the same process as the previous sample to obtain a mean maximum Zr concentration. For this sample, the eight highest analyses were averaged, providing a value of 77.2 (±12) ppm Zr. This created an error envelope that included all but one data point. Compared to the upper quartile mean of 74 ppm, the mean max Zr value better represents the peak conditions, though the two values are consistent within uncertainty. This value was used in the Zr-in-rutile equation to estimate a temperature range of 538° to 554°C ±12°C for pressures from 1.4 to 1.8 GPa, as shown in **Figure 12**.

SEC 29-2

Seventy analyses were conducted on sample SEC 29-2. The higher number is due to a transect taken of an individual large grain. The overall number of grains analyzed is roughly the same as the other samples. Of the 70 analyses, 22 were excluded. Only the four highest concentrations were needed to determine the mean maximum Zr concentration, as the error envelope included all but one analysis. The mean max Zr value was 92.3 (± 21) ppm Zr, consistent within uncertainty to the upper quartile mean of 82.6. For this sample in particular, the average obtained through the mean max Zr method appears to represent the highest temperature conditions better than an upper quartile mean would. Using this value, the peak metamorphic temperature of the sample was estimated to be 551° to 567°C ±19°C at pressures of 1.4 to 1.8 GPa, as shown in **Figure 12**.

An end-to-end transect of a single large rutile crystal in SEC 29-2 was obtained. Ten analyses were run on the crystal, starting on one end and measuring Zr concentrations towards the center of the crystal and then to the opposite end. The concentrations are presented in **Figure 11**. The Zr concentration of this crystal ranges from 38.5 ppm to 91.8 ppm. There does not appear to be a significant difference in concentration (within uncertainty) depending on location.

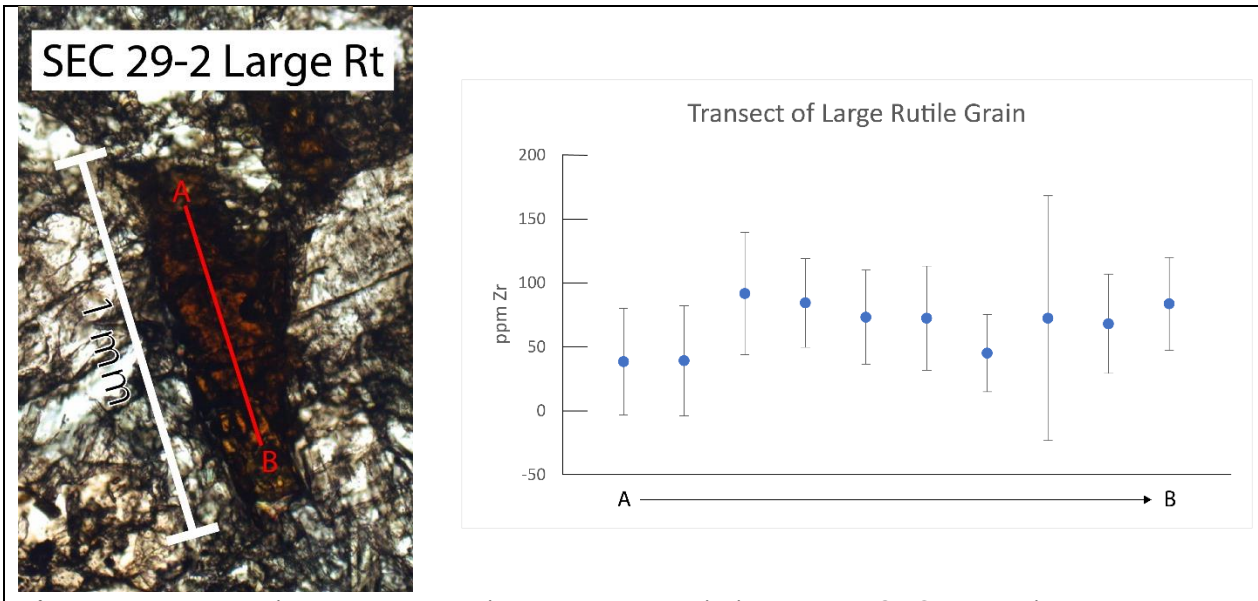

Figure 11: Photomicrograph showing the large grain in sample SEC 29-2 with the path of the transect from point A to point B overlain (left). Graph of Zr concentrations (with 2σ uncertainty) from point A to point B (right).

SEC 16-01

Sixty analyses were conducted on SEC 16-01. 20 were excluded, leaving 40 for analysis. The mean maximum Zr concentration was determined using the highest ten concentrations, producing a value of 79.9 (± 18) ppm Zr, comparable to the upper quartile value of 82.9. The uncertainty envelope contained all but five of the analyses. Using the mean max Zr value, the estimated temperature range for this sample was 540° to 556° ±19°C for pressures from 1.4 to 1.8 GPa, as shown in **Figure 12**.

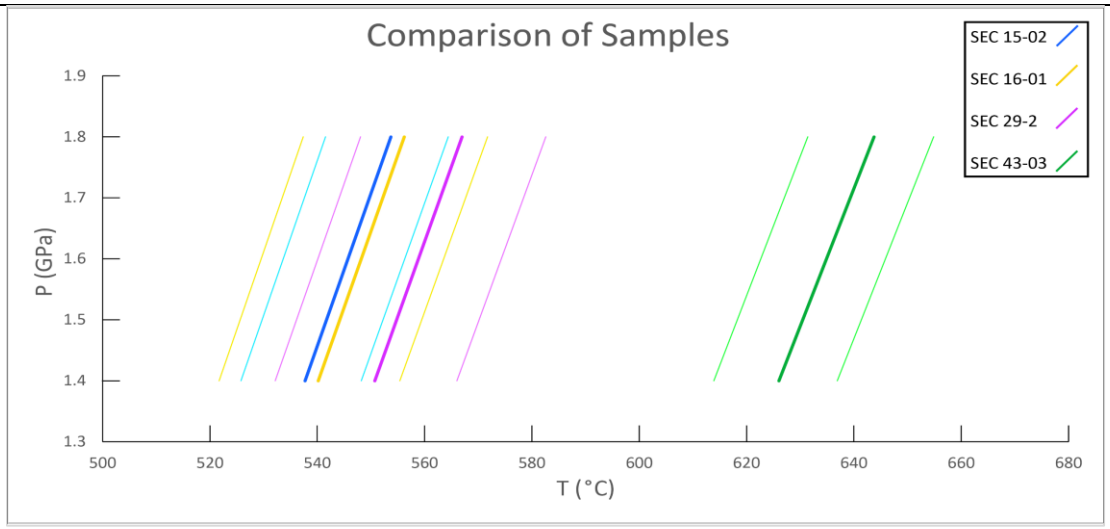

Figure 12: Estimated P-T conditions for samples based on the calculated mean max Zr concentration. Lower and upper bounds of uncertainty (2σ) are shown in lighter colors.

Discussion

Comparison

Zr-in-rutile temperature estimates for sample SEC 43-03 fall within the range of eclogite temperatures estimated by John et al. (2010), which showed a general range of 550-650°C for pressures from 1.6-1.8 GPa. At 1.6 GPa, the estimated temperature for this sample was 635°C. The estimated temperature at 1.8 GPa was 644°C. Sample SEC 29-2 also falls within the range of estimated eclogite temperatures, though it falls on the lower end of the range. At 1.6 GPa, the Zr-in-rutile estimated temperature was 559°C. At 1.8 GPa, the estimated temperature was 567°C. The margin of error does fall slightly outside of the expected range, with the lower bound at 532°C.

Though both samples are classed as eclogites due to the presence of omphacite and other high pressure/temperature minerals, there is a significant difference in their mineralogy. Sample SEC 43-03 contains little to no minerals typical in a blueschist, such as glaucophane or barroisite. SEC 29-2, however, does contain a significant amount of blue amphibole. This mineralogical difference provides further support for the difference in estimated temperatures as these mineral assemblages represent higher and lower P-T conditions, respectively.

Sample 15-02 falls within the overall expected blueschist temperature range of 500°-650°C at 1.4-1.6 GPa. At 1.4 GPa, the estimated temperature of SEC 15-02 was 538°C. At 1.6 GPa, the estimated temperature was 546°C. Sample 16-01 also falls within the expected range, displaying nearly identical temperatures to 15-02. At 1.4 GPa, the estimated temperature was 540°C. At 1.6 GPa, the estimated temperature was 548°C. These values are lower than those of the two eclogite samples, supporting the hypothesis that the blueschists would display lower temperatures than the eclogites.

A comparison of these results with the ranges estimated by John et al. (2010) is shown in **Figure 13**.

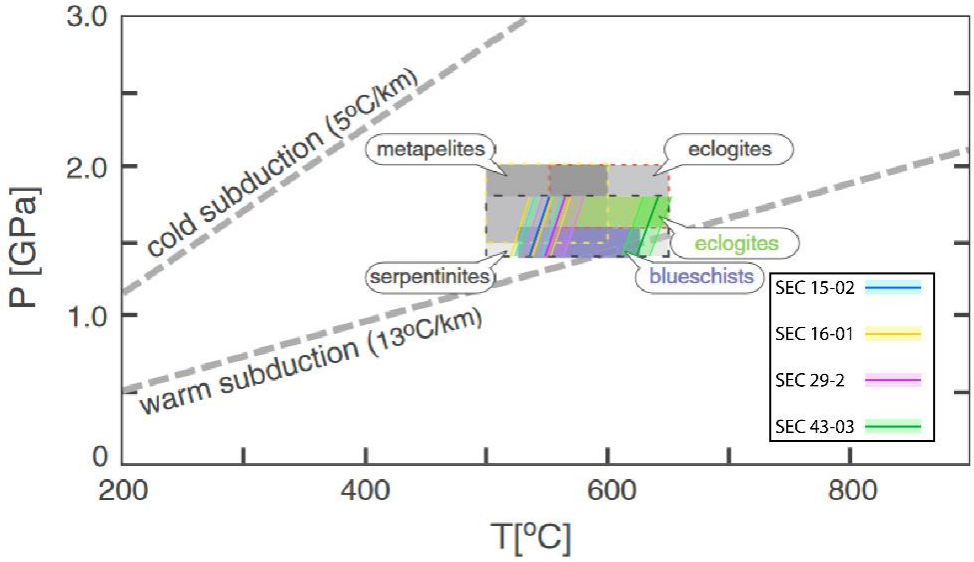

Figure 13: Estimated P-T conditions for samples SEC 15-02 (in blue), SEC 16-01 (in yellow), SEC 29-2 (in pink), and SEC 43-03 (in green) overlain on **Figure 10**. The uncertainty envelope for each is represented by the translucent box framed by opaque pale lines.

The estimates for these samples are also consistent with those analyzed by Guruvayurappan. The higher concentrations of Zr in rutile measured in sample SEC 43-03 are also present in sample SEC 43-1. For pressures of 1.6 to 1.8 GPa, the temperatures of sample SEC 43-1 range from 648°-657°C, while sample SEC 43-03 ranges from 635°-644°C. It is likely that these two thin sections were obtained from the same boulder. The three lower temperature eclogites are consistent within uncertainty. For pressures of 1.6 to 1.8 GPa, SEC 29-2 displays a temperature range of 559° to 567°C, SEC 27-1 displays a temperature range of 547° to 555°C, and SEC 50-01 displays a temperature range of 562° to 570°C. These samples likely represent the lowest temperatures of Raspas eclogites. The data for all five eclogites analyzed between these two studies was combined to create a field representing the overall temperature range estimated using the Zr-in-rutile thermometer. This field, along with a field combining the two blueschist estimates, is shown compared to the previous John et al. estimates in **Figure 14**.

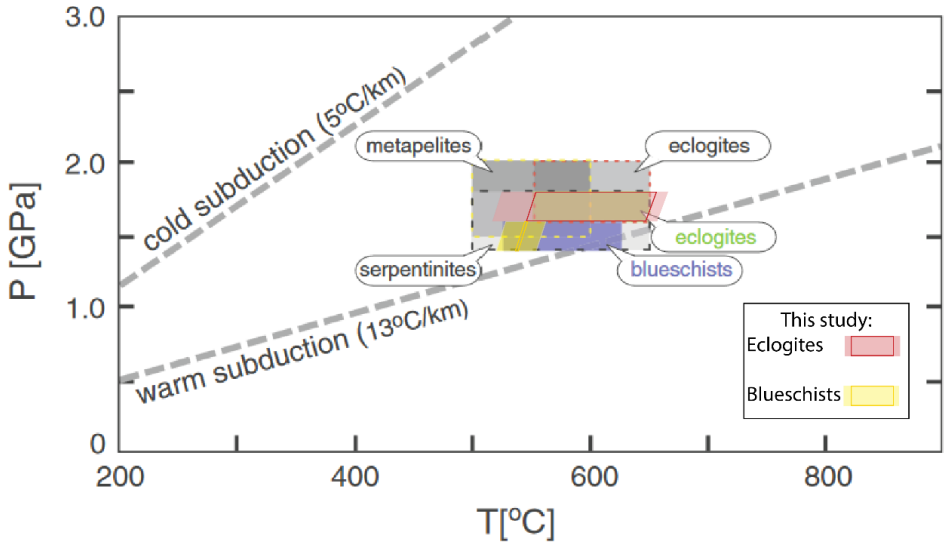

Figure 14: Combined temperature estimates for the seven samples analyzed overlain on **Figure 10**. The five eclogites are represented by the red region and the two blueschists are represented by the yellow region. The solid outlines encompass the calculated estimates, and the translucent fields represent the range between maximum uncertainties.

Garnet vs. Matrix

Zirconium concentrations of grains in garnet were compared with grains in the matrix to identify any correlations between location and recorded temperature. When a rutile forms as an inclusion in a garnet, the exchange of Zr for Ti is limited as the rock is uplifted. This could limit the effect of uplift, "freezing" the Zr concentration to that of the peak metamorphic temperature. For each sample, the range of Zr concentrations for each population was plotted as a box and whisker plot to visualize any notable differences between quartiles (**Figure 15**).

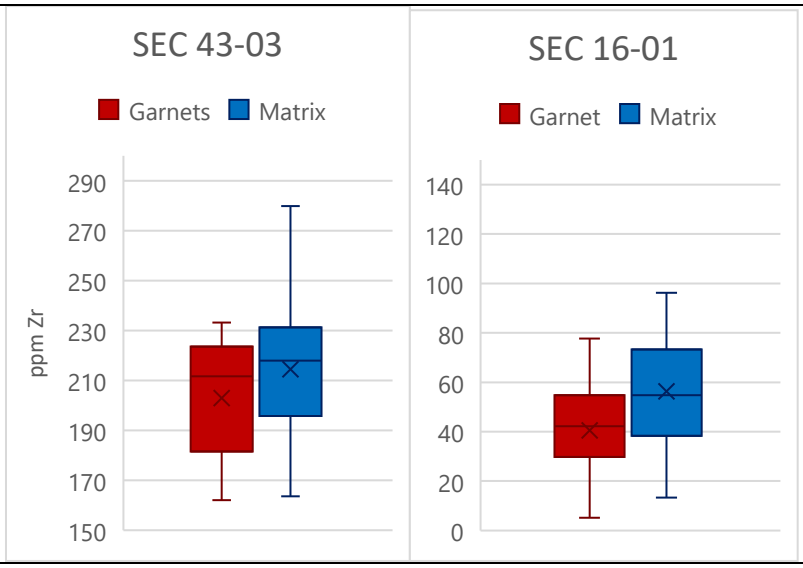

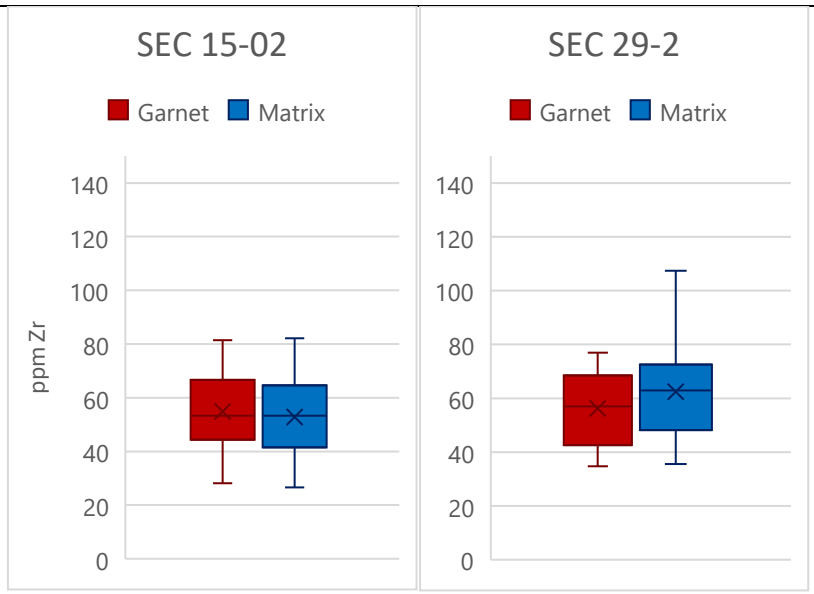

Figure 15: Box and whisker plots showing the distribution of Zr concentration values for different rutile grains in either the matrix or in garnet.

In SEC 43-03, 12 analyses were rutile grains included in garnet. The median Zr concentration of the matrix rutile was 218 ppm, while the median of the garnet rutile was 212 ppm. The means were 215 ppm and 203 ppm respectively. For SEC 15-02, 22 of the 48 valid analyses were rutile in garnet. The median and mean Zr concentration of matrix rutile were 53.3 ppm and 52.9 ppm, while the median of rutile in garnet were 53.3 ppm and 54.9 ppm. In SEC 16-01, 14 of the 40 analyses were rutile in garnet. The median Zr concentration in the matrix was 54.8 ppm and the mean concentration was 56.4 ppm. The median concentration in garnet was 42.2 ppm with a mean of 40.5 ppm. Unfortunately, many of the analyses on rutile crystals in garnet were excluded from the dataset for SEC 29-2. This left only nine analyses of the 48 as rutile in garnet. The median and mean of the concentration in the matrix were 62.9 ppm and 62.4 ppm. The median and mean of the concentration in garnet were 57.0 ppm and 56.3 ppm.

Based on these comparisons, there does not appear to be a difference in Zr concentrations in rutile whether it is found in the matrix or included in garnet in these samples. This suggests that either the garnet did not preserve the rutile during uplift as expected or that there was not much retrograde substitution of Zr into the rutile.

Suggestions for Future Work

The two unused samples, the three samples studied by Guruvayurappan, and sample SEC 43-03 have been sent to the University of South Carolina for further study. The remaining three samples analyzed in this study will be sent as well. Researchers there will be using geobarometry to estimate the specific pressure conditions for each sample. The pressure estimates can then be combined with the temperatures estimated in this study to determine the precise P-T conditions for each sample. Future work should also include

building new numerical models of the Andean subduction zone in this region of Ecuador. The detailed pressure and temperature conditions from this study and others like it can be used to improve the constraints of the models to hopefully better understand the differences between predicted and estimated temperatures.

In continuing this study, it would be useful to obtain samples from other subduction zones, both fossil and active, for comparison. It would be interesting to see the differences in temperature depending on the subduction zone, as the Raspas Complex appears to represent a warm one (John et al., 2010).

Conclusions

The goal of this study is to determine the peak temperature conditions experienced by eclogites and blueschists from the Raspas Complex in southwestern Ecuador, a metamorphic accretionary complex formed in the Late Jurassic due to the subduction of the Nazca plate under South America. The results of this study are useful in understanding the conditions within this subduction zone, providing insight into the processes occurring there. The null hypothesis that Zr-in-rutile temperature estimates will be consistent with previous results is supported. As expected, eclogite samples displayed higher temperatures than blueschist samples. Eclogite samples recorded a temperature range of 559° to 644°C for pressures of 1.6 to 1.8 GPa, while blueschist samples displayed temperatures of 538° to 548°C at pressures of 1.4 to 1.6 GPa. For these samples, there does not appear to be a correlation between recorded temperature and location of rutile within garnet or matrix. Further study of these samples and comparing their results to samples from additional locations will provide a greater understanding of the nature of subduction zones.

Acknowledgements

Thank you to Dr. Penniston-Dorland for advising me on this project and to Christiana Hoff, Kathy Stepien, and Kate Bickerstaff for offering their advice throughout the semester. Thank you to Dr. Piccoli for assistance with the electron probe and the overall process of Senior Thesis. I would also like to thank Dr. Timm John and his team for collecting and providing these samples and Srinidhi Guruvayurappan for her analysis of samples 27-1, 43-1, and 50-01.

Bibliography

Bosch, D., Gabriele, P., Lapierre, H., Malfere, J.-L., & Jaillard, E. (2002). Geodynamic significance of the Raspas Metamorphic Complex (SW Ecuador): Geochemical and isotopic constraints. *Tectonophysics*, *345*(1–4), 83–102. https://doi.org/10.1016/S0040-1951(01)00207-4

Feininger, T. (1980). Eclogite and Related High-Pressure Regional Metamorphic Rocks from the Andes of Ecuador. *Journal of Petrology*, *21*(1), 107–140. https://doi.org/10.1093/petrology/21.1.107

Gabriele, P. (n.d.). *HP terranes exhumation in active margin setting: Geology, petrology and geochemistry of the Raspas Complex in SW Ecuador*.

Gerya, T. V., Stöckhert, B., & Perchuk, A. L. (2002). Exhumation of high-pressure metamorphic rocks in a subduction channel: A numerical simulation. *Tectonics*, *21*(6). https://doi.org/10.1029/2002TC001406

Harvey, K. M., Penniston-Dorland, S. C., Kohn, M. J., & Piccoli, P. M. (2021). Assessing *P-T* variability in mélange blocks from the Catalina Schist: Is there differential movement at the subduction interface? *Journal of Metamorphic Geology*, *39*(3), 271–295. https://doi.org/10.1111/jmg.12571

Jaillard, E., Soler, P., Carlier, G., & Mourier, T. (1990). Geodynamic evolution of the northern and central Andes during early to middle Mesozoic times: A Tethyan model. *Journal of the Geological Society*, *147*(6), 1009–1022. https://doi.org/10.1144/gsjgs.147.6.1009

John, T., Scherer, E. E., Schenk, V., Herms, P., Halama, R., & Garbe-Schönberg, D. (2010). Subducted seamounts in an eclogite-facies ophiolite sequence: The Andean Raspas Complex, SW Ecuador. *Contributions to Mineralogy and Petrology*, *159*(2), 265–284. https://doi.org/10.1007/s00410-009-0427-0

Kohn, M. J. (2020). A refined zirconium-in-rutile thermometer. *American Mineralogist*, *105*(6), 963–971. https://doi.org/10.2138/am-2020-7091

Penniston-Dorland, S. C., Kohn, M. J., & Manning, C. E. (2015). The global range of subduction zone thermal structures from exhumed blueschists and eclogites: Rocks are hotter than models. *Earth and Planetary Science Letters*, *428*, 243–254. https://doi.org/10.1016/j.epsl.2015.07.031

Penniston-Dorland, S. C., Kohn, M. J., & Piccoli, P. M. (2018). A mélange of subduction temperatures: Evidence from Zr-in-rutile thermometry for strengthening of the subduction interface. *Earth and Planetary Science Letters*, *482*, 525–535. https://doi.org/10.1016/j.epsl.2017.11.005

Syracuse, E. M., Van Keken, P. E., & Abers, G. A. (2010). The global range of subduction zone thermal models. *Physics of the Earth and Planetary Interiors*, *183*(1–2), 73–90. https://doi.org/10.1016/j.pepi.2010.02.004

Tomkins, H. S., Powell, R., & Ellis, D. J. (2007). The pressure dependence of the zirconium-in-rutile thermometer. *Journal of Metamorphic Geology*, *25*(6), 703–713. https://doi.org/10.1111/j.1525-1314.2007.00724.x

Ueda, H., 2016, High-pressure, low-temperature metamorphism, Encyclopedia of Earth Sciences, p. 311–316, doi:10.1007/978-94-007-6238-1_113.

Van Keken, P. E., & Wilson, C. R. (2023). An introductory review of the thermal structure of subduction zones: I—motivation and selected examples. *Progress in Earth and Planetary Science*, *10*(1), 42. https://doi.org/10.1186/s40645-023-00573-z

Winter, J. D. (2014). *Principles of igneous and metamorphic petrology* (2. ed., Pearson new internat. ed). Pearson Education.

Zack, T., Moraes, R., & Kronz, A. (2004). Temperature dependence of Zr in rutile: Empirical calibration of a rutile thermometer. *Contributions to Mineralogy and Petrology*, *148*(4), 471–488. https://doi.org/10.1007/s00410-004-0617-8

Appendices

Appendix 1. Scans of samples

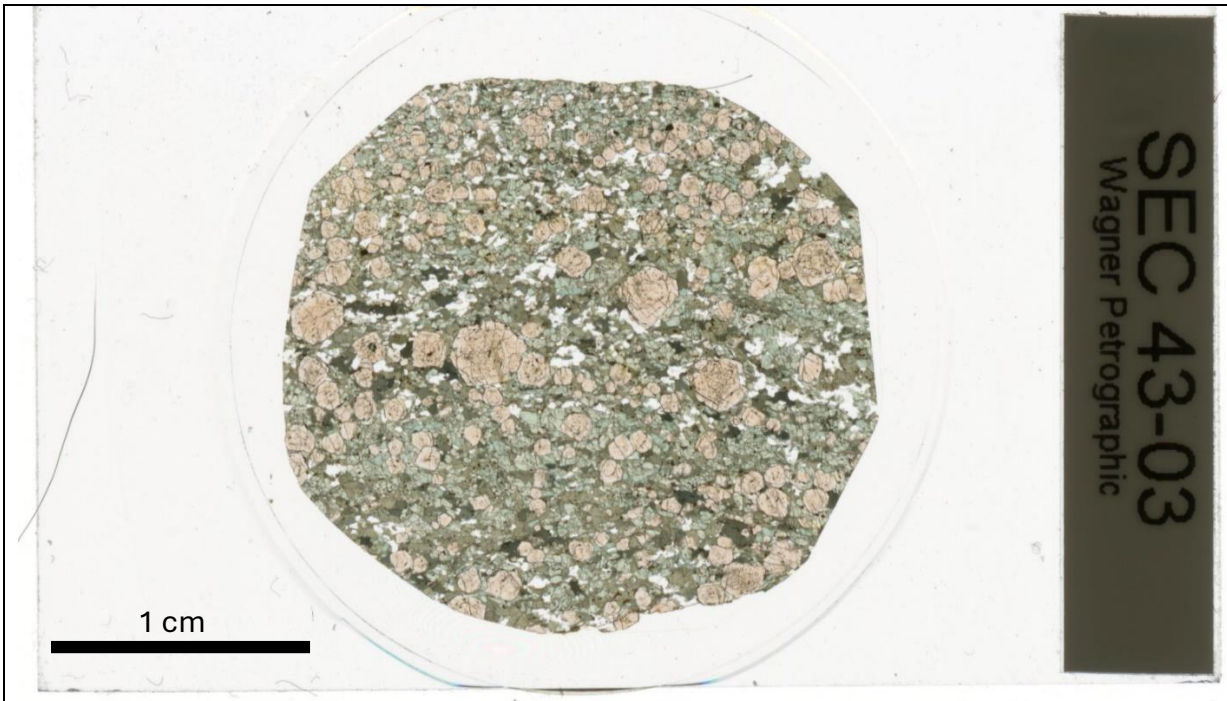

Figure A-1: A scan of sample SEC 43-03.

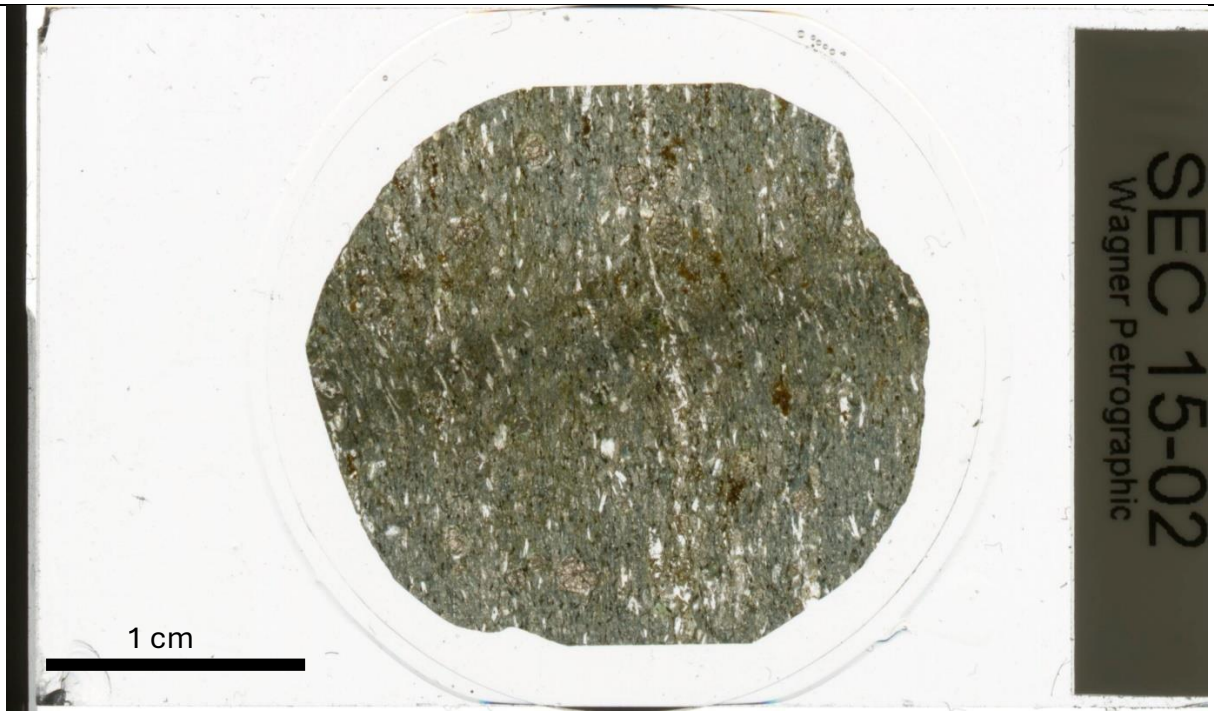

Figure A-2: A scan of sample SEC 15-02

Figure A-3: A scan of sample SEC 29-2.

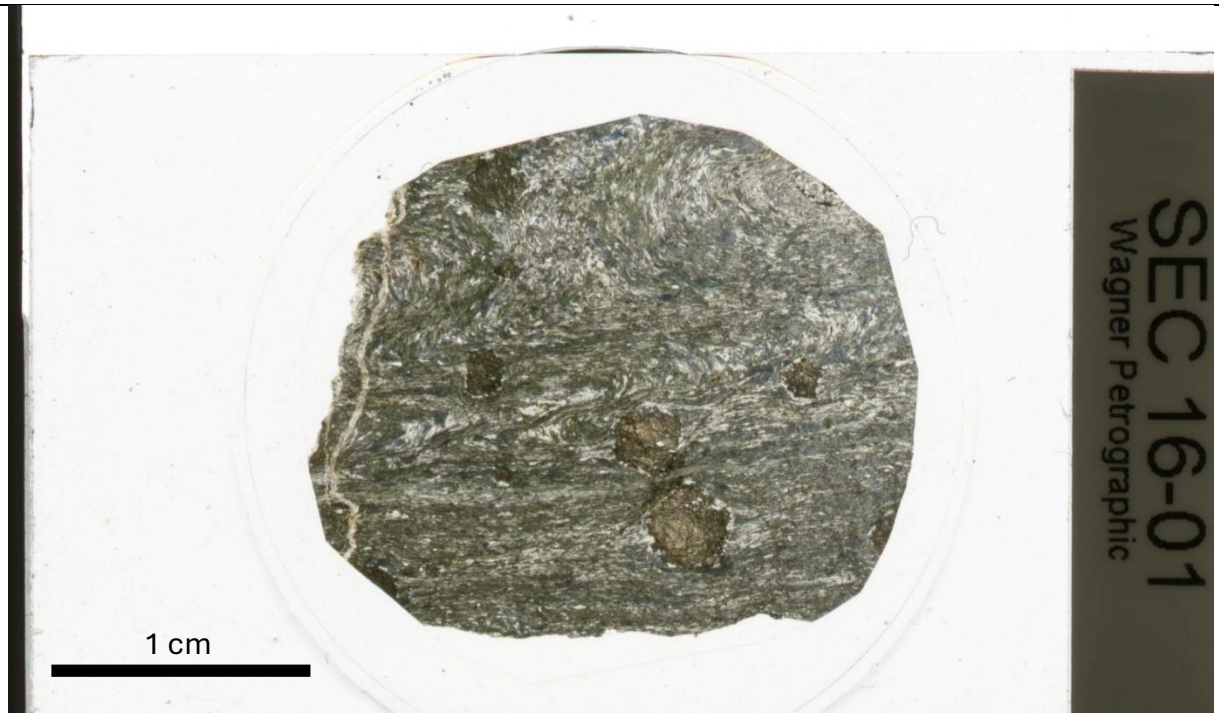

Figure A-4: A scan of sample SEC 16-01.

Appendix 2. WDS data

Raw data from the EPMA for sample SEC 43-03. Analyses 1-5 record data for standard K-13-02. Analyses 6-52 represent various locations on SEC 43-03.

Table A-1.

No.	TiO2	ZrO2	Al2O3	FeO	Nb2O5	SiO2	Cr2O3	MnO	Ta2O5	V2O3	Total	ZrO2 unc (1σ)
1	98.62	0.0405	0.11	0.46	0.19	-0.01	0.19	0.00	0.04	0.39	100.03	6.32
2	98.27	0.0348	0.12	0.40	0.12	-0.02	0.24	0.01	0.04	0.40	99.62	6.91
3	98.54	0.0376	0.12	0.44	0.13	-0.01	0.18	-0.03	-0.02	0.39	99.78	6.81
4	98.65	0.0393	0.11	0.41	0.16	-0.02	0.25	0.00	-0.07	0.39	99.92	6.76
5	98.19	0.0359	0.17	0.40	0.14	-0.01	0.18	0.00	-0.07	0.41	99.44	6.81
6	98.99	0.0268	0.10	0.54	0.02	-0.01	0.03	0.03	-0.01	0.40	100.13	8.72
7	98.32	0.0264	0.09	0.65	0.00	-0.01	0.00	-0.02	-0.08	0.39	99.36	9.32
8	99.06	0.0281	0.12	0.61	0.00	-0.02	0.06	-0.03	0.05	0.35	100.23	8.91
9	99.36	0.0323	0.11	0.53	0.00	-0.01	0.04	-0.05	0.01	0.38	100.41	7.32
10	98.24	0.0378	0.12	0.53	0.01	-0.01	0.05	0.01	-0.05	0.37	99.29	6.23
11	97.74	0.0321	0.20	0.48	0.00	-0.01	0.05	-0.01	0.08	0.38	98.93	6.44
12	98.46	0.0344	0.10	0.53	0.01	0.00	0.01	-0.01	0.00	0.38	99.51	6.61
13	97.57	0.0252	0.08	0.64	0.03	-0.01	0.01	-0.02	0.01	0.40	98.74	9.51
14	98.10	0.0294	0.07	0.58	0.02	-0.01	0.10	-0.01	-0.04	0.36	99.19	8.86
15	98.30	0.0299	0.09	0.58	0.05	-0.01	0.05	-0.02	-0.02	0.39	99.43	7.38
16	95.51	0.0339	0.11	0.47	0.00	-0.01	0.09	0.04	-0.02	0.45	96.67	7.19
17	97.88	0.0279	0.10	0.51	0.04	-0.01	0.07	0.03	-0.03	0.38	99.01	7.71
18	98.25	0.0302	0.09	0.52	0.01	-0.01	0.03	0.00	-0.05	0.40	99.27	8.12
19	97.36	0.0266	0.13	0.54	0.04	-0.01	0.04	0.03	-0.02	0.39	98.52	9.27
20	96.15	0.0315	0.14	0.54	0.04	0.27	0.08	0.02	-0.02	0.37	97.62	7.09
21	98.88	0.0293	0.11	0.58	0.02	-0.02	0.04	0.01	0.04	0.30	100.00	7.87
22	93.29	0.0298	0.12	3.36	0.04	-0.01	0.01	0.05	0.01	0.38	97.27	7.35
23	98.53	0.0328	0.10	0.50	0.04	-0.01	0.00	0.02	-0.05	0.45	99.64	7.18
24	99.63	0.0294	0.10	0.56	0.02	-0.02	0.07	-0.03	-0.02	0.36	100.70	8.07
25	97.95	0.0308	0.07	0.60	0.02	-0.02	0.06	-0.01	-0.07	0.43	99.07	6.82
26	96.38	0.0212	0.08	0.85	0.01	-0.01	0.02	0.01	0.00	0.43	97.78	11.54
27	98.65	0.0322	0.09	0.62	0.02	-0.01	0.01	-0.01	0.03	0.36	99.80	6.71
28	99.10	0.0251	0.08	0.39	0.00	-0.02	0.04	0.00	-0.08	0.43	99.95	9.77
29	97.25	0.0318	0.10	0.66	0.03	-0.01	0.02	0.00	-0.03	0.38	98.43	7.4
30	98.61	0.0302	0.09	0.66	-0.01	-0.02	0.04	0.02	-0.01	0.40	99.82	7.45
31	98.63	0.0243	0.09	0.75	0.03	-0.02	0.06	0.00	-0.07	0.37	99.87	10.04
32	98.34	0.0314	0.09	0.62	-0.01	-0.02	0.11	0.02	-0.08	0.36	99.46	6.92
33	100.14	0.0295	0.08	0.56	0.03	0.00	0.14	0.02	-0.02	0.44	101.42	7.42
34	99.76	0.0221	0.09	0.54	0.02	0.00	0.10	0.02	-0.01	0.38	100.93	8.64
35	98.76	0.0304	0.09	0.68	0.02	-0.01	0.06	0.01	-0.01	0.44	100.07	6.99
36	98.03	0.0279	0.10	0.66	0.05	-0.02	0.00	-0.01	-0.02	0.42	99.24	8.3

No.	TiO2	ZrO2	Al2O3	FeO	Nb2O5	SiO2	Cr2O3	MnO	Ta2O5	V2O3	Total	ZrO2 Unc (1σ)
37	99.60	0.0308	0.08	0.52	0.02	-0.02	0.14	0.00	-0.11	0.40	100.67	7.1
38	98.94	0.0302	0.08	0.72	0.00	-0.02	0.03	0.01	0.03	0.42	100.23	7.51
39	98.36	0.0219	0.09	0.86	0.00	-0.01	0.05	-0.02	-0.06	0.46	99.74	9.59
40	98.54	0.0256	0.11	0.65	0.01	-0.01	0.07	0.02	0.03	0.37	99.81	8.61
41	98.50	0.0224	0.12	0.62	0.01	-0.01	0.05	0.01	0.01	0.32	99.65	11.21
42	98.30	0.0315	0.08	0.59	0.01	-0.01	0.05	-0.02	-0.07	0.34	99.31	6.92
43	98.69	0.0264	0.08	0.46	0.00	-0.01	0.15	-0.03	-0.04	0.48	99.81	7.54
44	98.00	0.0295	0.07	0.48	0.02	-0.01	0.26	0.01	0.06	0.48	99.39	7.71
45	98.41	0.0241	0.06	0.38	-0.01	0.02	0.24	-0.02	-0.01	0.59	99.69	8.11
46	98.61	0.0257	0.07	0.51	0.03	-0.01	0.22	-0.02	-0.01	0.46	99.88	8.4
47	98.65	0.0298	0.07	0.53	0.05	-0.01	0.23	-0.01	0.00	0.42	99.95	7.16
48	97.90	0.0195	0.06	1.16	0.03	-0.01	0.05	0.01	-0.05	0.41	99.58	12.69
49	97.37	0.0180	0.06	1.73	0.01	0.00	0.17	0.01	0.03	0.42	99.80	11.8
50	98.85	0.0258	0.09	0.46	0.03	-0.01	0.15	0.00	-0.04	0.45	99.99	7.57
51	98.44	0.0296	0.06	0.48	0.02	-0.01	0.16	-0.02	-0.02	0.41	99.54	7.21
52	98.63	0.0274	0.07	0.41	0.01	-0.01	0.13	-0.02	-0.04	0.42	99.63	6.56

Raw data from the EPMA for sample SEC 15-02. Analyses 1-5 record data for a standard K-13-02. Analyses 6-58 represent various locations on SEC 15-02.

Table A-2.

No.	TiO2	ZrO2	Al2O3	FeO	Nb2O5	SiO2	Cr2O3	MnO	Ta2O5	Total	ZrO2 Unc (1σ)
1	98.403	0.036	0.117	0.473	0.111	-0.016	0.204	-0.007	-0.042	99.279	6.8
2	98.431	0.040	0.163	0.404	0.130	-0.013	0.239	0.016	0.050	99.461	6.8
3	98.575	0.035	0.140	0.490	0.107	-0.019	0.204	0.018	-0.058	99.491	8.6
4	98.415	0.034	0.141	0.452	0.110	-0.015	0.173	0.007	0.002	99.318	7.2
5	97.777	0.036	0.117	0.429	0.127	-0.017	0.214	0.016	-0.011	98.688	6.4
6	99.061	0.008	0.111	0.846	0.134	0.078	0.133	0.022	-0.079	100.314	39.6
7	98.240	0.008	0.114	0.524	0.137	0.121	0.135	0.033	0.040	99.351	39.5
8	94.198	2.692	0.103	0.497	0.122	1.015	0.090	0.030	-0.072	98.673	0.2
9	99.537	0.009	0.116	0.471	0.136	-0.020	0.119	0.031	-0.011	100.388	31.2
10	97.833	0.004	0.110	0.532	0.122	-0.002	0.095	-0.009	-0.019	98.665	39.4
11	99.614	0.004	0.123	0.559	0.116	-0.007	0.077	0.049	0.046	100.580	72.7
12	98.403	0.006	0.113	0.679	0.107	-0.014	0.050	0.013	0.041	99.398	42.8
13	100.062	0.007	0.111	0.579	0.148	-0.005	0.069	0.022	0.033	101.027	40.0
14	99.608	0.009	0.116	0.646	0.134	0.001	0.119	-0.009	0.029	100.651	37.8
15	99.609	0.007	0.111	0.631	0.115	-0.016	0.078	0.017	-0.038	100.517	74.6
16	99.814	0.011	0.121	0.779	0.114	-0.009	0.116	0.007	0.046	100.998	30.6
17	100.696	0.006	0.127	0.791	0.099	-0.010	0.103	-0.017	0.054	101.849	33.3

No.	TiO2	ZrO2	Al2O3	FeO	Nb2O5	SiO2	Cr2O3	MnO	Ta2O5	Total	ZrO2 Unc (1σ)
18	98.096	0.009	0.123	0.867	0.112	-0.013	0.083	-0.015	0.040	99.304	25.8
19	98.678	0.010	0.132	0.831	0.113	-0.008	0.066	0.023	-0.003	99.842	71.1
20	99.026	0.010	0.116	0.736	0.137	0.022	0.111	-0.023	0.025	100.158	31.5
21	99.637	0.009	0.124	0.520	0.107	-0.010	0.096	0.036	-0.032	100.485	33.7
22	99.318	0.008	0.139	0.749	0.142	0.020	0.103	0.035	-0.005	100.509	45.5
23	98.457	0.006	0.132	0.787	0.147	0.052	0.127	-0.003	-0.004	99.700	37.5
24	98.893	0.007	0.111	0.521	0.167	-0.009	0.101	0.006	0.006	99.803	35.4
25	99.948	0.004	0.129	0.452	0.148	-0.016	0.102	0.014	-0.070	100.711	68.2
26	99.613	0.007	0.119	0.447	0.115	-0.025	0.112	-0.022	-0.025	100.340	31.0
27	99.140	0.007	0.114	0.490	0.128	-0.011	0.104	-0.014	0.051	100.010	66.4
28	99.689	0.007	0.119	0.433	0.122	-0.015	0.097	0.024	-0.023	100.452	31.6
29	99.344	0.005	0.110	0.429	0.122	-0.006	0.082	-0.002	-0.039	100.044	45.3
30	99.682	0.006	0.123	0.874	0.139	-0.009	0.173	0.012	-0.013	100.986	38.0
31	96.696	0.012	0.199	0.771	0.128	0.174	0.207	0.031	-0.022	98.195	31.4
32	99.399	0.010	0.120	0.735	0.113	-0.006	0.074	-0.013	0.041	100.472	26.2
33	96.013	0.004	0.123	3.966	0.130	-0.004	0.129	0.638	-0.011	100.989	57.2
34	100.058	0.007	0.104	0.547	0.122	-0.018	0.116	-0.016	0.014	100.935	44.4
35	99.252	0.007	0.108	0.523	0.163	-0.009	0.105	-0.004	0.025	100.170	34.2
36	100.002	0.008	0.131	0.428	0.133	-0.011	0.108	-0.015	-0.037	100.746	32.8
37	99.578	0.008	0.108	0.426	0.132	-0.013	0.134	-0.006	-0.007	100.361	35.5
38	98.039	0.010	0.133	0.546	0.117	-0.008	0.088	0.025	-0.084	98.864	104.6
39	99.097	0.011	0.124	0.488	0.101	-0.008	0.105	0.004	-0.059	99.864	42.9
40	99.881	0.005	0.106	0.383	0.133	-0.026	0.109	-0.004	-0.058	100.529	66.1
41	99.855	0.006	0.127	0.470	0.127	-0.018	0.115	-0.013	0.012	100.679	167.0
42	99.494	0.006	0.128	0.596	0.144	-0.017	0.148	0.011	-0.012	100.497	41.9
43	99.032	0.006	0.152	0.926	0.139	0.071	0.132	-0.007	-0.007	100.444	110.6
44	99.436	0.007	0.144	0.719	0.131	-0.010	0.163	0.030	0.014	100.635	61.7
45	99.209	0.005	0.145	0.805	0.141	-0.010	0.147	0.020	-0.047	100.414	78.6
46	99.782	0.007	0.133	0.766	0.122	0.003	0.168	0.043	-0.030	100.995	45.4
47	100.280	0.007	0.126	0.675	0.154	0.009	0.139	0.025	0.048	101.463	47.9
48	100.698	0.008	0.135	0.645	0.120	0.112	0.126	0.027	0.053	101.922	31.0
49	100.224	0.009	0.127	0.725	0.110	0.013	0.101	0.005	-0.033	101.279	21.5
50	98.004	0.007	0.152	1.066	0.087	0.017	0.164	0.063	0.007	99.567	37.5
51	100.275	0.011	0.130	0.569	0.127	-0.018	0.160	0.018	-0.055	101.217	45.7
52	100.373	0.004	0.127	0.651	0.124	-0.019	0.115	0.001	0.025	101.401	1322.9
53	99.889	0.004	0.131	0.739	0.119	-0.014	0.130	0.033	-0.036	100.995	69.5
54	100.828	0.005	0.141	0.857	0.133	-0.009	0.164	0.019	0.015	102.154	65.4
55	99.722	0.006	0.128	0.429	0.123	-0.010	0.089	0.013	0.003	100.503	39.4

No.	TiO2	ZrO2	Al2O3	FeO	Nb2O5	SiO2	Cr2O3	MnO	Ta2O5	Total	ZrO2 Unc (1σ)
56	100.221	0.009	0.144	0.411	0.095	-0.012	0.107	-0.009	-0.023	100.942	24.7
57	98.055	0.009	0.127	0.412	0.102	-0.018	0.088	0.010	-0.036	98.749	46.6
58	99.966	0.006	0.131	0.459	0.133	-0.006	0.079	0.027	-0.077	100.718	49.3

Raw data from the EPMA for sample SEC 29-2.

Table A-3.

No.	TiO2	ZrO2	Al2O3	FeO	Nb2O5	SiO2	Cr2O3	MnO	Ta2O5	Total	ZrO2 Unc (1σ)
117	100.003	0.009	0.120	0.444	0.275	-0.023	0.062	0.038	-0.034	100.894	27.8
118	100.656	0.007	0.126	0.504	0.284	-0.021	0.054	-0.017	0.027	101.620	45.6
119	100.384	0.005	0.111	0.377	0.257	-0.033	0.059	0.022	-0.022	101.160	185.1
120	100.599	0.005	0.108	0.681	0.242	-0.030	0.040	-0.021	-0.013	101.610	81.1
121	99.334	0.010	0.123	1.101	0.210	0.025	0.069	0.027	-0.034	100.867	23.6
122	99.159	0.009	0.160	1.245	0.215	0.036	0.069	0.017	0.062	100.972	50.3
123	100.024	0.012	0.171	0.345	0.273	-0.022	0.106	-0.004	-0.044	100.862	27.8
124	98.120	0.009	0.157	0.318	0.212	-0.017	0.042	-0.021	-0.030	98.789	45.6
125	99.897	0.006	0.179	0.307	0.298	-0.003	0.067	-0.034	-0.035	100.682	185.1
126	98.538	0.009	0.148	0.371	0.253	-0.016	0.070	-0.037	-0.085	99.251	81.1
127	100.468	0.007	0.174	0.412	0.231	-0.016	0.075	-0.013	-0.003	101.336	22.2
128	99.765	0.007	0.148	0.443	0.220	-0.017	0.112	-0.016	-0.063	100.598	52.6
129	99.866	0.010	0.134	0.324	0.234	-0.022	0.116	-0.009	-0.022	100.631	30.3
130	99.507	0.008	0.129	0.582	0.257	-0.022	0.108	-0.009	-0.020	100.538	20.5
131	99.410	0.010	0.154	0.319	0.267	-0.019	0.120	-0.012	0.010	100.259	26.3
132	99.998	0.009	0.181	0.318	0.282	-0.019	0.090	-0.012	0.007	100.853	44.1
133	99.934	0.008	0.144	0.778	0.246	-0.016	0.070	0.025	0.012	101.200	39.6
134	99.537	0.007	0.148	0.782	0.244	-0.013	0.028	0.035	-0.027	100.740	27.6
135	99.141	0.009	0.126	0.347	0.228	-0.016	0.105	0.029	-0.039	99.931	54.5
136	98.062	0.008	0.151	0.355	0.209	-0.015	0.106	-0.001	-0.080	98.796	32.5
137	97.653	0.005	0.139	0.286	0.254	-0.017	0.072	-0.020	0.001	98.373	43.9
138	99.652	0.005	0.152	0.425	0.170	-0.025	0.072	0.008	-0.002	100.457	34.3
139	100.206	0.012	0.173	0.364	0.168	-0.021	0.052	-0.006	-0.032	100.917	25.8
140	100.325	0.011	0.139	0.286	0.191	-0.027	0.068	0.019	-0.002	101.011	34.0
141	99.494	0.010	0.159	0.289	0.218	-0.022	0.095	0.021	0.036	100.300	54.0
142	99.622	0.010	0.146	0.374	0.205	-0.020	0.087	-0.010	0.037	100.450	54.9
143	99.900	0.006	0.200	0.368	0.185	-0.015	0.038	-0.001	-0.006	100.674	26.0
144	100.321	0.010	0.168	0.240	0.196	-0.019	0.057	-0.031	-0.049	100.893	20.5
145	100.287	0.009	0.181	0.339	0.206	-0.023	0.091	0.001	0.026	101.116	25.1
146	99.865	0.011	0.153	0.272	0.173	-0.011	0.070	0.015	0.009	100.557	28.0

No.	TiO2	ZrO2	Al2O3	FeO	Nb2O5	SiO2	Cr2O3	MnO	Ta2O5	Total	ZrO2 Unc (1σ)
147	98.884	0.011	0.161	1.062	0.368	0.034	0.071	0.051	0.201	100.843	33.4
148	99.565	0.011	0.140	1.003	0.373	-0.003	0.063	0.022	-0.039	101.134	65.9
149	43.654	0.001	13.820	16.569	0.078	21.631	0.018	0.522	0.039	96.332	28.5
150	93.354	0.012	1.982	2.823	0.165	2.788	0.027	0.070	-0.063	101.156	21.8
151	72.216	0.004	8.298	8.978	0.133	12.156	0.017	0.331	-0.016	102.117	26.2
152	96.377	0.013	1.178	1.785	0.203	1.469	0.032	0.062	0.018	101.135	45.1
153	45.784	0.002	11.859	15.421	0.119	18.886	0.021	0.361	0.078	92.531	59.2
154	1.785	-0.001	21.188	26.735	0.014	36.328	-0.004	0.596	-0.026	86.615	20.5
155	99.960	0.009	0.163	0.828	0.213	0.011	0.071	-0.010	0.008	101.254	91.1
156	55.061	0.002	0.656	0.759	0.101	20.412	0.023	0.000	0.006	77.021	22.0
157	78.217	0.004	0.339	0.568	0.173	10.441	0.065	0.045	0.008	89.859	409.8
158	99.998	0.009	0.152	0.621	0.216	0.038	0.062	0.040	0.035	101.170	100.0
159	100.348	0.007	0.150	0.386	0.168	-0.017	0.047	-0.006	-0.035	101.047	25.8
160	101.269	0.007	0.171	0.396	0.161	-0.026	0.042	0.002	0.051	102.073	180.9
161	100.259	0.007	0.154	0.270	0.173	-0.020	0.042	-0.006	-0.019	100.860	281.0
162	101.603	0.010	0.165	0.298	0.207	-0.020	0.047	-0.005	0.011	102.316	31.3
163	99.562	0.007	0.187	1.263	0.203	0.019	0.042	0.040	-0.056	101.267	32.4
164	8.951	0.001	19.771	25.106	0.038	33.023	0.014	0.730	-0.057	87.575	34.6
165	52.335	0.002	10.707	13.370	0.119	16.703	0.041	0.447	-0.046	93.678	40.4
166	99.991	0.013	0.162	1.046	0.196	0.008	0.039	0.019	-0.058	101.414	28.8
167	100.230	0.009	0.136	0.808	0.192	-0.006	0.089	-0.011	0.032	101.480	18.4
168	99.818	0.010	0.151	0.893	0.197	-0.011	0.085	0.017	0.056	101.216	100.0
169	95.844	0.011	0.130	2.845	0.264	-0.004	0.085	0.070	0.004	99.248	124.8
170	99.312	0.011	0.151	1.048	0.283	0.001	0.082	0.006	0.049	100.942	20.3
171	99.869	0.007	0.145	0.907	0.215	-0.007	0.058	0.035	0.033	101.262	20.6
172	52.608	0.001	9.203	10.780	0.124	16.248	0.017	0.295	0.004	89.279	33.5
173	99.495	0.016	0.177	1.051	0.196	0.109	0.090	0.010	0.017	101.161	20.7
174	99.951	0.011	0.173	1.004	0.254	0.000	0.065	-0.003	0.039	101.493	29.1
175	100.520	0.005	0.088	0.289	0.201	-0.017	0.096	0.023	0.002	101.207	82.2
176	100.102	0.008	0.133	0.300	0.195	-0.017	0.071	0.009	0.067	100.867	55.5
177	101.230	0.010	0.140	0.300	0.236	-0.012	0.080	-0.007	0.008	101.985	16.8
178	100.210	0.007	0.133	0.302	0.255	-0.021	0.089	-0.019	0.021	100.977	26.2
179	100.406	0.006	0.141	0.311	0.238	-0.020	0.083	-0.008	-0.009	101.148	37.8
180	100.120	0.010	0.158	0.259	0.244	-0.019	0.092	-0.010	0.013	100.867	32.4
181	100.258	0.005	0.181	0.283	0.253	-0.001	0.085	-0.011	0.055	101.107	19.6
182	99.201	0.015	0.231	0.276	0.228	0.180	0.080	0.022	-0.031	100.201	51.7
183	100.267	0.011	0.101	0.241	0.226	-0.018	0.061	-0.006	0.089	100.972	33.2
184	101.175	0.006	0.121	0.236	0.284	-0.018	0.086	0.005	-0.009	101.886	93.1

Raw data from the EPMA for sample SEC 16-01.

Table A-4.

No.	TiO2	ZrO2	Al2O3	FeO	Nb2O5	SiO2	Cr2O3	MnO	Ta2O5	Total	ZrO2 Unc (1σ)
1	98.633	0.0328	0.1155	1.0012	0.1815	0.0103	0.1217	-0.0061	0.0111	100.1009	7.0
2	98.0983	0.0101	0.125	1.3396	0.1804	-0.008	0.1391	0.1082	-0.0716	99.9211	31.4
3	97.3048	0.0076	0.1414	1.006	0.2006	-0.0132	0.1076	-0.0078	0.0346	98.7817	38.0
4	98.4036	0.0087	0.1257	1.0348	0.1756	0.0011	0.1259	0.0014	-0.0215	99.8554	24.8
5	98.4978	0.0046	0.1299	0.9484	0.1398	-0.0088	0.1321	0.0161	-0.0105	99.8495	30.4
6	98.4404	0.0055	0.1203	0.999	0.1392	-0.0024	0.1157	0.0132	-0.0155	99.8154	47.8
7	98.5393	0.0074	0.1304	0.7362	0.1398	-0.0045	0.0863	0.0209	-0.0015	99.6544	23.0
8	97.6976	0.0013	0.1168	0.758	0.113	-0.0124	0.098	-0.021	0.0309	98.7822	239.6
9	97.2029	0.0057	0.1196	1.9432	0.1917	-0.0215	0.0799	0.2076	0.0362	99.7654	40.4
10	97.5207	0.0059	0.1223	1.3652	0.163	-0.0092	0.0869	0.1033	0.0189	99.3771	33.9
11	97.1836	0.006	0.1247	1.3474	0.1885	-0.0156	0.0901	0.0816	0.0446	99.0509	34.4
12	98.8358	0.0007	0.1243	0.7012	0.1637	-0.0059	0.1242	-0.0059	-0.0215	99.9167	95.2
13	98.0391	0.1953	0.1309	1.7078	0.1453	0.0915	0.0959	0.0626	0.0383	100.5066	1.4
14	73.5882	0.0029	0.6128	22.6345	0.1336	0.9888	0.0739	2.9001	0.031	100.9657	48.8
15	98.531	0.0038	0.1276	0.7084	0.1342	-0.0148	0.163	-0.0063	0.0037	99.6507	149.2
16	98.431	0.0059	0.1394	0.7243	0.1715	0.008	0.1951	-0.0021	-0.0531	99.62	38.6
17	98.2871	0.0091	0.143	0.8209	0.2333	0.0004	0.1074	0.0132	-0.0911	99.5233	29.5
18	97.9299	0.0059	0.1478	0.8752	0.1932	-0.0028	0.1373	0.0158	0.0357	99.338	90.5
19	97.0235	0.013	0.1273	1.0335	0.1943	0.0171	0.1448	0.0233	-0.0807	98.4961	15.8
20	96.3403	0.0059	0.1381	1.0317	0.1821	0.0061	0.1835	0.0113	-0.0135	97.8856	41.1
21	98.4702	0.0105	0.1373	0.6106	0.1839	-0.0123	0.0755	0.0012	0.0299	99.5069	25.7
22	98.6468	0.0052	0.1205	0.5596	0.1594	-0.0134	0.0732	0.0118	0.01	99.5732	33.5
23	98.4383	0.0087	0.1365	0.5766	0.2134	-0.0011	0.1179	0.0238	0.0561	99.5703	41.6
24	98.3327	0.0051	0.1419	0.5756	0.182	0.0017	0.0743	-0.0353	0.0063	99.2844	33.3
25	98.6772	0.0058	0.141	0.6281	0.1697	-0.0099	0.109	0.0151	0.0283	99.7643	38.0
26	98.4403	0.0088	0.1494	0.5977	0.1498	-0.0106	0.0712	0.0058	-0.0551	99.3574	24.3
27	98.6639	0.0086	0.1396	0.451	0.2025	-0.0103	0.081	-0.0185	0.0351	99.553	28.1
28	98.2922	0.0042	0.1632	0.4432	0.1311	-0.0086	0.1032	0.0094	-0.031	99.107	108.5
29	98.9156	0.0057	0.1371	0.4713	0.1662	-0.0126	0.0619	-0.0204	0.053	99.7778	32.4
30	98.9007	0.0071	0.1325	0.5723	0.2129	-0.0118	0.1004	0.0005	0.0173	99.932	26.5
31	98.6474	0.0119	0.1257	0.5818	0.2163	-0.0128	0.0724	0.0012	-0.001	99.643	21.2
32	99.9894	0.0117	0.1273	0.5535	0.2076	-0.0133	0.0541	0.0074	-0.0405	100.8972	21.7
33	98.8437	0.0077	0.1261	0.4898	0.1806	-0.0172	0.0755	0.0202	-0.0205	99.706	26.8
34	99.2944	0.005	0.1311	0.5294	0.1789	-0.0123	0.0892	-0.0269	0.0168	100.2056	100.0
35	97.6039	0.0071	0.137	0.5357	0.2034	-0.009	0.0588	0.0062	-0.0731	98.4701	35.5

No.	TiO2	ZrO2	Al2O3	FeO	Nb2O5	SiO2	Cr2O3	MnO	Ta2O5	Total	ZrO2 Unc (1σ)
36	98.8776	0.0092	0.1421	0.5157	0.1512	-0.0123	0.0397	0.0062	-0.0321	99.6974	20.6
37	98.0443	0.0042	0.1383	0.55	0.1507	-0.0172	0.074	-0.0074	-0.1062	98.8308	28.7
38	97.6967	0.1255	0.1381	0.6047	0.1297	0.0652	0.0534	0.0029	-0.0055	98.8108	2.1
39	99.1128	0.0044	0.1397	0.8068	0.1726	-0.0087	0.0837	-0.0046	0.0189	100.3256	114.0
40	98.8446	0.0011	0.1195	0.8272	0.145	-0.0136	0.1004	0.0223	-0.0641	99.9824	2301.3
41	99.1684	0.0041	0.1461	0.5263	0.16	-0.0079	0.0821	-0.0292	-0.0545	99.9955	270.6
42	98.6066	0.0077	0.1386	0.5175	0.1775	-0.0106	0.0643	-0.0034	-0.0356	99.4627	38.0
43	98.7592	0.006	0.1426	0.9149	0.1618	-0.0081	0.1057	0.0101	-0.0125	100.0796	24.3
44	98.6136	0.0074	0.1434	0.9427	0.1772	-0.0087	0.1356	0.0254	-0.02	100.0166	55.1
45	94.5539	0.0074	0.1464	4.9371	0.1746	-0.0015	0.1265	0.4907	-0.017	100.4181	31.4
46	98.9971	0.0039	0.1473	1.1484	0.146	-0.0102	0.1512	0.0552	-0.0486	100.5902	34.8
47	98.1975	0.013	0.1359	0.4818	0.1821	-0.015	0.0837	0.0058	0.0042	99.0891	17.5
48	96.8901	0.0069	0.1421	1.2652	0.1132	-0.0087	0.094	0.0334	0.0068	98.543	103.9
49	99.1159	0.0065	0.1213	0.4199	0.137	-0.0097	0.0756	-0.0137	0.0131	99.866	36.6
50	98.9199	0.0018	0.1312	0.439	0.1504	-0.0173	0.097	-0.0015	0.033	99.7535	132.7
51	98.8568	0.0097	0.1373	0.466	0.1252	-0.01	0.1071	-0.009	-0.0205	99.6626	48.4
52	99.0795	0.0064	0.1341	0.6757	0.1366	-0.0034	0.1086	0.0341	-0.0185	100.153	21.2
53	92.7339	0.0271	0.1496	5.3512	0.1408	0.0169	0.1045	0.8198	0.0016	99.3455	8.9
54	83.4136	0.0462	0.1511	13.437	0.1558	0.325	0.1006	2.143	0.0031	99.7754	5.6
55	98.3566	0.0041	0.1438	0.7984	0.2191	-0.012	0.1203	0.0077	0.0315	99.6695	60.5
56	98.2813	0.0105	0.1511	0.9294	0.1353	-0.0159	0.0856	0.0581	-0.0561	99.5794	33.4
57	0.024	-1.3488	0.083	0.0307	0.003	-0.2105	-0.0065	-0.0012	-0.1689	-1.5951	100.0
58	0.0297	-1.6981	0.0119	0.0838	-0.0077	-0.2592	-0.0022	0.0207	-0.0244	-1.8455	100.0
59	97.654	0.0114	0.1529	0.5496	0.1842	-0.0072	0.0708	-0.0046	0.0089	98.62	24.3
60	98.8747	0.0109	0.1321	0.5605	0.2119	-0.0039	0.0587	0.0079	0.012	99.8649	21.5

Appendix 3. Mean Max Zr graphs

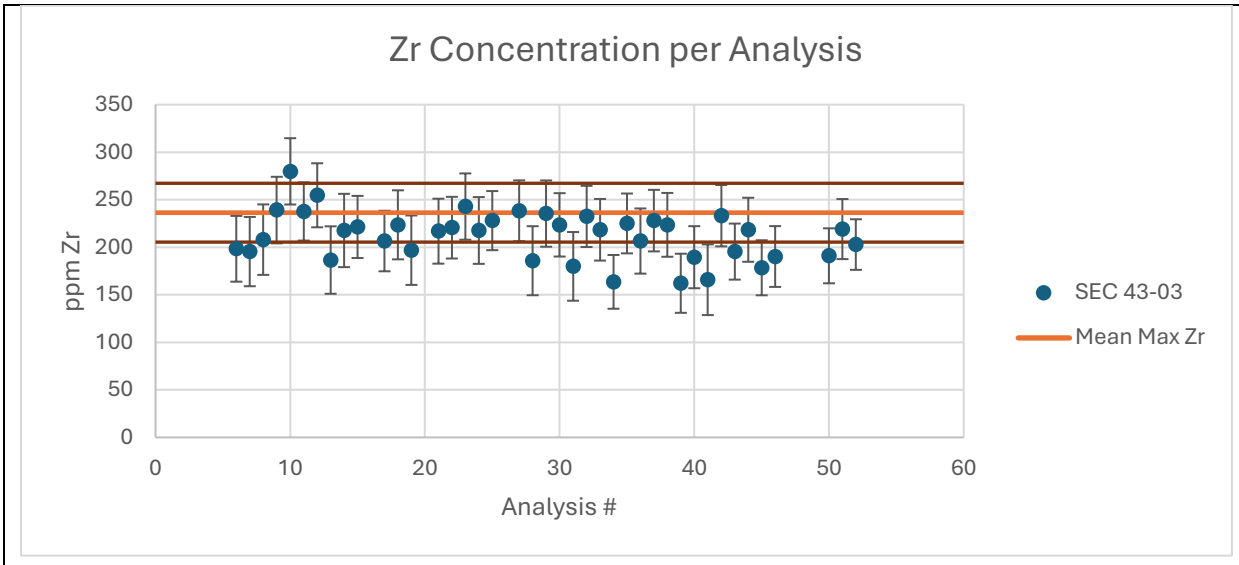

Figure A-5: Individual Zr concentrations for SEC 43-03. The orange line represents the calculated mean maximum Zr value. The brown lines represent the 2σ error envelope.

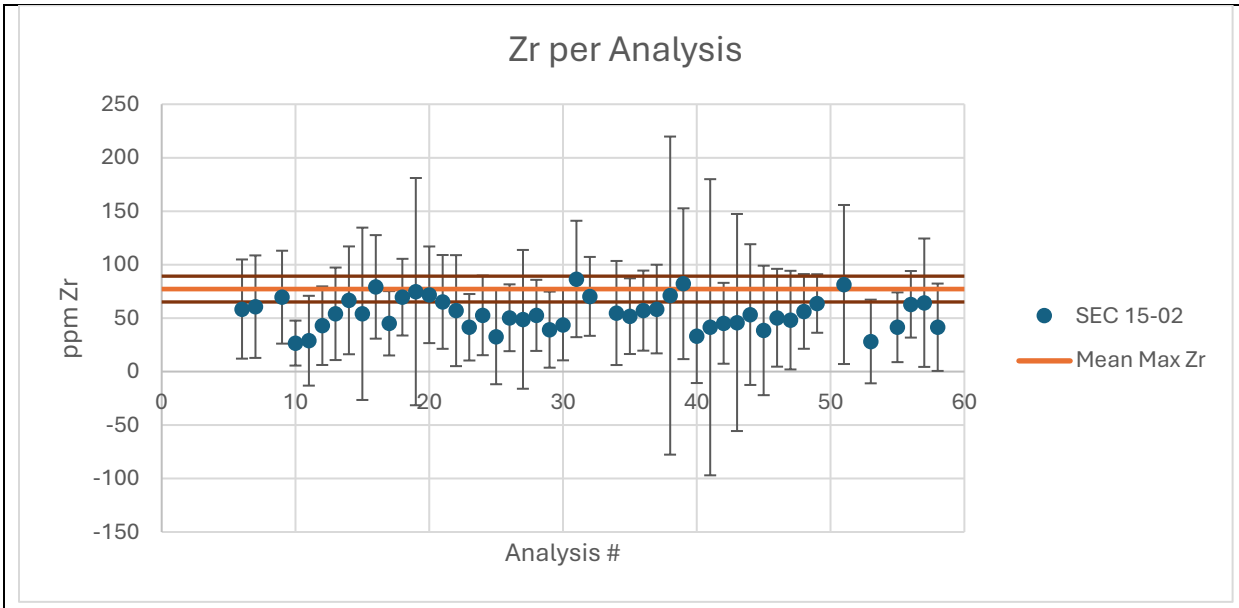

Figure A-6: Individual Zr concentrations for SEC 15-02. The orange line represents the calculated mean maximum Zr value. The brown lines represent the 2σ error envelope.

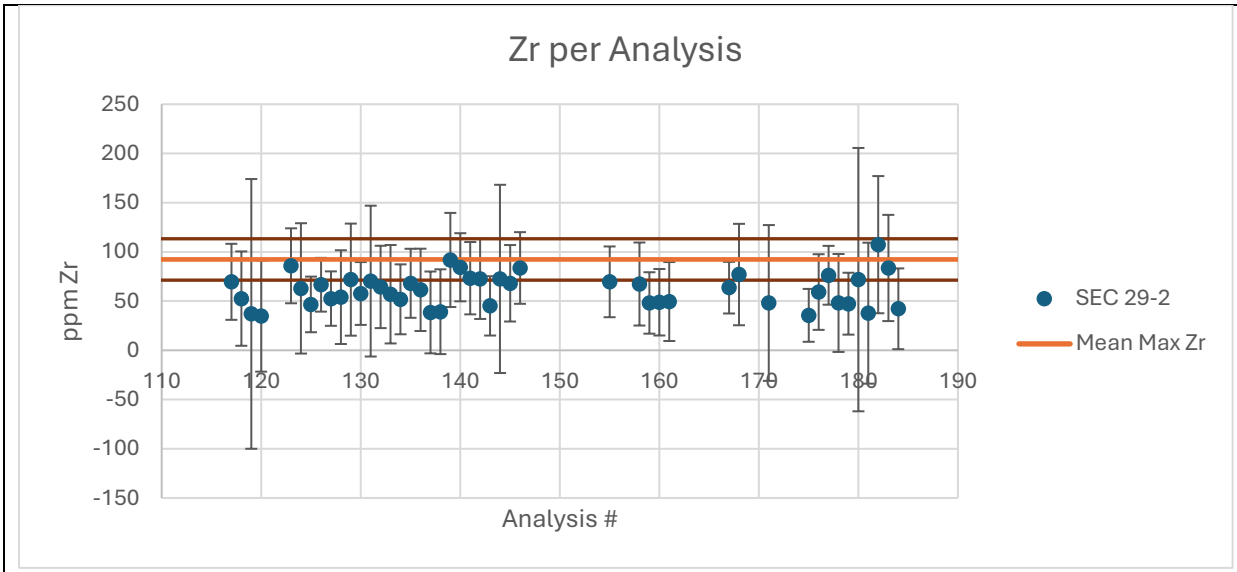

Figure A-7: Individual Zr concentrations for SEC 29-2. The orange line represents the calculated mean maximum Zr value. The brown lines represent the 2σ error envelope.

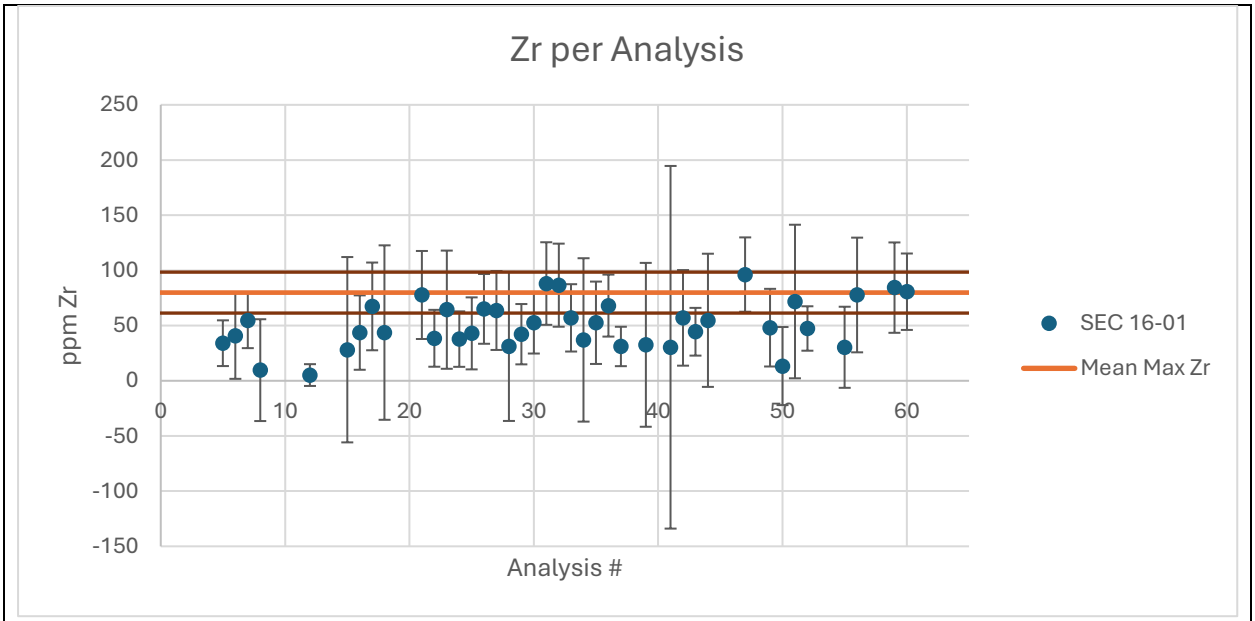

Figure A-8: Individual Zr concentrations for SEC 16-01. The orange line represents the calculated mean maximum Zr value. The brown lines represent the 2σ error envelope.

Appendix 4. Data from previous study

Table provided by Srinidhi Guruvayurappan based on her data from Summer 2023.

Table A-5.

Sample	Zr (ppm)	UNC U	UNC L	Pressure(bars)	Temp	Temp Unc U	Temp Unc L
SEC 27-1	78.08	104.31	51.86	13000	534.55	555.64	506.48
SEC 27-1	78.08	104.31	51.86	14000	538.55	559.75	510.35
SEC 27-1	78.08	104.31	51.86	15000	542.55	563.86	514.21
SEC 27-1	78.08	104.31	51.86	16000	546.56	567.97	518.08
SEC 27-1	78.08	104.31	51.86	17000	550.56	572.08	521.94
SEC 27-1	78.08	104.31	51.86	18000	554.56	576.18	525.80
SEC 43-1	274.04	303.32	244.77	13000	634.62	643.79	624.63
SEC 43-1	274.04	303.32	244.77	14000	639.12	648.34	629.08
SEC 43-1	274.04	303.32	244.77	15000	643.62	652.88	633.53
SEC 43-1	274.04	303.32	244.77	16000	648.12	657.43	637.98
SEC 43-1	274.04	303.32	244.77	17000	652.63	661.98	642.43
SEC 43-1	274.04	303.32	244.77	18000	657.13	666.52	646.88
SEC 50-01	96.49	118.83	74.15	13000	549.86	565.50	530.89
SEC 50-01	96.49	118.83	74.15	14000	553.94	569.65	534.87
SEC 50-01	96.49	118.83	74.15	15000	558.01	573.81	538.86
SEC 50-01	96.49	118.83	74.15	16000	562.09	577.97	542.84
SEC 50-01	96.49	118.83	74.15	17000	566.17	582.12	546.83
SEC 50-01	96.49	118.83	74.15	18000	570.25	586.28	550.81

Appendix 5. Honor Pledge

I pledge on my honor that I have not given or received any unauthorized assistance or plagiarized on this assignment.